Monthly element/Ca trends and inter chamber variability in two planktic Foraminifera species: *Globigerinoides ruber albus* and *Turborotalita clarkei* from a hypersaline oligotrophic sea

Noy Levy[1,2], Adi Torfstein[1,3], Ralf Schiebel[2], Natalie Chernihovsky[1,3], Klaus Peter Jochum[2] ✝, Ulrike Weis[2], Brigitte Stoll[2], Gerald H. Haug[2,4]

1) The Fredy & Nadine Herrmann Institute of Earth Sciences, Hebrew University of Jerusalem, Jerusalem 91904, Israel.
2) Max Planck Institute for Chemistry, Hahn-Meitner-Weg 1, 55128 Mainz, Germany.
3) Interuniversity Institute for Marine Sciences, Eilat 88103, Israel.
4) Department of Earth Sciences, ETH Zurich, Sonneggstrasse 5, 8092 Zurich, Switzerland
✝ Deceased, November 9, 2024

Correspondence to: Noy Levy (noy.levy2@mail.huji.ac.il)

Abstract

Environmental and biological factors influence the trace element composition (element/Ca) of planktic foraminifer shells. Consequently, the element/Ca measured in these shells (tests) are utilized as proxies to reconstruct past oceanic and climatic conditions. As single shell analyses are increasingly used in paleoceanographic research it is important to understand how proxy systematics change between species, individuals of the same species in a given population, and among chambers of a single individual during its life cycle. Here we present a time series of the chemical composition of planktic foraminifers retrieved using sediment traps between June 2014 and June 2015 at the northern part of the Gulf of Aqaba (aka Gulf of Eilat). Laser ablation ICP-MS element/Ca measurements were performed on single shells and chambers of *Globigerinoides ruber albus* and *Turborotalita clarkei*, collected monthly from five water depths (120 m, 220 m, 350 m, 450 m, and 570 m). Sediment trap samples were paired with corresponding data on water column hydrography and chemistry. Pooled means of measured element/Ca display species-specific and element-specific behavior, with generally higher

values for *T. clarkei* phenotypes ('big' and 'encrusted') in comparison to *G. ruber albus*. Some element/Ca values measured in water column specimens, such as Al/Ca, vary significantly from core-top specimens. A unique finding is a prominent increase in element/Ca around March-April 2015, during maximum water column mixing, mostly apparent in *T. clarkei* and to a lesser extent in *G. ruber albus*. This spring element/Ca increase is observed in most measured elements and is further associated with an increase in inter-chamber variability (ICV). Inter-chamber element/Ca patterns show element enrichment/depletion in the most recently precipitated (final, F0) chamber in comparison to the older chambers (penultimate (F-1), antepenultimate (F-2), etc.). Element/Ca in F0 may also be less sensitive to surrounding environmental conditions. For example, the Mg/Ca of the F-1 and F-2 chambers of *G. ruber albus* display a positive relationship with mixed layer temperatures while F0 does not. To overcome this effect, we suggest using pooled means from non-F0 fractions as environmental records and paleo proxies.

These results highlight the complexity of proxy systematics that rises from the variability in element/Ca measured among different species and between chambers, caused by ecological conditions and other processes in the water column including physical, chemical, and biological effects.

1. Introduction

1.1 Planktic foraminifera as traces of the past environment

Planktic Foraminifera (PF) shells are useful archives for studying the history of Earth's climate and oceans, as their calcareous shells reflect the environmental conditions during their formation (Berggren et al., 1995; Rosenthal, 2007; Schiebel & Hemleben, 2017; Kucera, 2007; Katz et al., 2010; Gupta, 1999; Davis et al., 2020,). Various element/Ca measured in PF tests have been linked to ambient seawater temperature (e.g., Mg/Ca; Nurenberg et al., 1996; Rosenthal et al., 2004), salinity (e.g., Na/Ca; Mezger et al., 2016; Gray et al., 2023), the carbonate system (e.g., B/Ca; Babila et al., 2014; Henehan et al., 2015; Haynes et al., 2019), productivity (e.g., Ba/Ca; Fritz-Enders et al., 2022), and chemical weathering (e.g., Ti/Ca; Amaglio et al., 2025). In the past, the use of these proxies relied on bulk analysis of the entire shell or multiple shells. However, although first attempts in single chamber LA-ICP-MS started back in 2003 (Eggins et al., 2003, Reichart et al., 2003), only in recent years there has been an increase in the use of high-resolution analytical techniques, such as Laser Ablation (LA) ICP-

MS and electron microprobe analyses in paleoceanographic studies (Davis et al., 2020). The element/Ca measurements of single specimens (Individual Foraminifer Analysis, IFA) revealed high variability between individuals of the same population as well as significant intra-shell variability (i.e., inter chamber variability, ICV) (Sadekov et al., 2008; Fehrenbacher et al., 2020; Hupp & Fehrenbacher, 2024; Fischer et al., 2024; Davis et al., 2020, and references therein). Despite the analytical advancements, the variations in the geochemical signatures of PF shells are poorly understood and while they are likely related to the life cycles and reproductive modes of many species there are still knowledge gaps in our understanding of proxy systematics in single shell and single chamber of PF species. There is also a lack of detailed description and understanding of element/Ca systematics in description of small-sized species such as *T. clarkei*, which have been largely overlooked in previous studies despite their significant contribution to the settling PF tests (export flux), as observed in the northern Red Sea (Chernihovsky et al., 2018). Furthermore, specific marine regions, such as in oligotrophic, subtropical basins, particularly in deep-water environments, are not well-established in terms of their spatial and temporal dynamics (Schiebel & Hemleben, 2017).

1.2 Planktic Foraminifer population dynamics in The Gulf of Aqaba

The Gulf of Aqaba (GOA) is considered an open ocean proxy environment (Chase et al., 2011). It is an oligotrophic basin where the main lithogenic flux is derived from dust. During summer (April-September), a ~200 m deep thermocline separates nutrient-depleted surface waters (~25°C) from the nutrient-rich deep layer (~21°C). In winter-spring (October-April), the thermocline gradually erodes due to surface cooling (Figs. 1a and 1e; Meeder et al., 2012), which can lead to the development of a deep mixed layer. Although the depth of the mixed layer varies annually with climatic conditions, the long-term mean mixing depth is approximately 300-400 m, and deep mixing can extend to the sea floor while it typically reaches maximum depth by late March. The regional terrestrial climate is hyper-arid (mean annual rainfall <30 mm) and the main sources for terrigenous material to the GOA are dust storms originating from the Sahara and Arabian Deserts, as well as rare localized floods (Katz et al., 2015; Chase et al., 2011; Ganor et al., 2001; Torfstein et al., 2017).

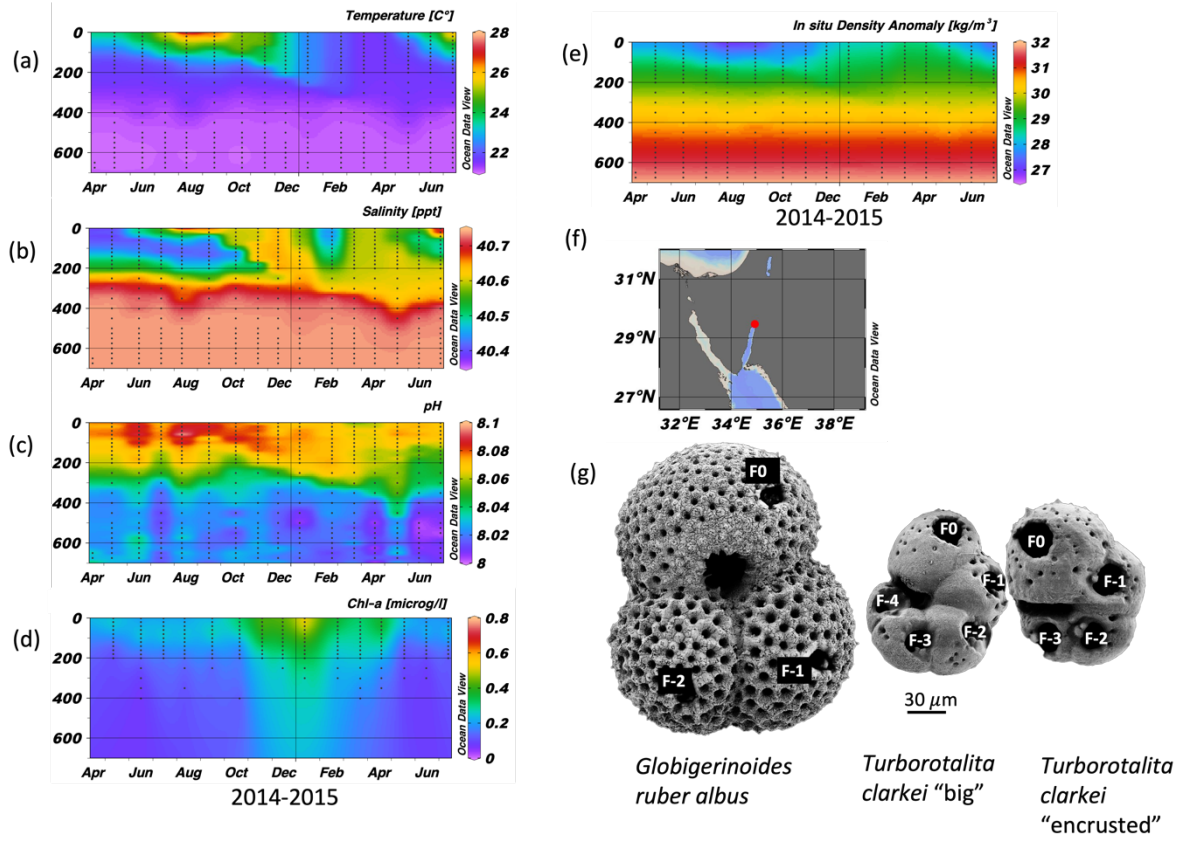

Figure 1: Time series of temperature (a), salinity (b), *p*H (c), Chlorophyll-a concentration (d), and in situ density anomaly (e), measured in the Gulf of Aqaba between April 2014 and June 2015 by the National Monitoring Program (NMP, Shaked & Genin, 2016). Y-axis is depth (m); A map of the Gulf of Aqaba (f); and (g) scanning electron micrographs of the three morpho-species (exhibiting ablation holes in each chamber (labelled), from Levy et al., 2023).

Planktic foraminifera fluxes in the GOA demonstrate strong seasonality, with low fluxes during the summer months, gradually increasing during the autumn-winter, coeval with decreasing sea-surface temperatures and deepening of the mixed layer in the GOA that drives advection of nutrient-replete subsurface waters into the mixed layer (Fig. 2). This in turn triggers an increase in primary productivity, expressed by enhanced chlorophyll-a concentrations and higher PF fluxes (Chernihovsky et al., 2018, 2020).

Spinose species constitute the majority of the PF assemblage. The smaller size fraction, 63-125 μm, is 86% from the total flux and is dominated by *T. clarkei.* The 125-500 μm size-fraction (~13 %) is dominated by the species *G. ruber albus*, while less than 1% of the shells are in the range of 500-1000 μm, dominated by *O. universa* (Chernihovsky et al., 2018).

Globigerinoides ruber albus and *T. clarkei* inhabit different dwelling-depths and have different life strategies. *Globigerinoides ruber albus* is a surface dweller and is photo-symbiont

bearing, while *T. clarkei* tends to dwell below the mixed layer depth and is barren of photo-symbionts (Rebotim et al., 2017; Schiebel & Hemleben, 2017; Levy et al., 2023). Furthermore, it has been suggested that *G. ruber albus* and *T. clarkei* do not share the same dietary preferences: *G. ruber albus* being more carnivorous than the detritivorous *T. clarkei* which may forage at the exported matter below the pycnocline (Schiebel & Hemleben, 2017). In the GOA, *T. clarkei* has two phenotypes: *T. clarkei* 'big', with all of its test chambers are fully recognizable and their surface is relatively smooth and *T. clarkei* 'encrusted' with a less smooth shell surface and is smaller than the 'big' type (Levy et al., 2023).

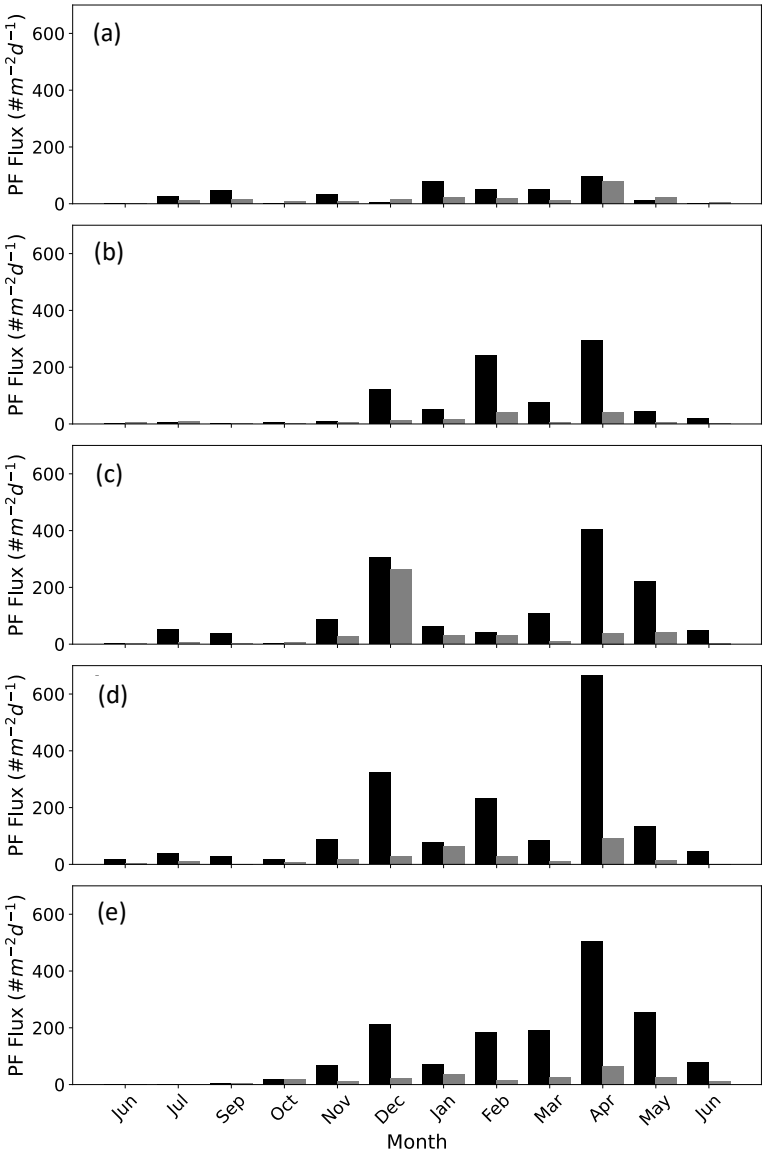

Figure 2: PF fluxes in the Gulf of Aqaba between June 2014 and June 2015 presented according to the size fractions >63-125 µm (black bars) and >125-500 µm (grey bars) at the different sediment trap depths a) 120 m, b) 220 m, c) 340 m, d) 450 m, and e) 570 m. Data from Chernihovsky et al. (2018).

In this study, we investigate the range of element values, year-round trends and inter-chamber element/Ca variability in *G. ruber albus* and *T. clarkei* tests collected in sediment traps at various water column depths from the GOA. We assess whether the chambers record temporal-seasonal patterns, and the implications for using single chamber data for geochemical proxies (Mg/Ca, B/Ca, Na/Ca). Examining inter-chamber variability sheds light on how trace elements are incorporated during calcification, distinguishing physiological controls (e.g., ontogenetic changes across successive chambers) from environmental influences such as temperature, salinity and nutrient availability. Using *G. ruber* and *T. clarkei* from the GOA provides a contrasting framework which together, these species enable us to refine element/Ca proxy calibrations across vertical gradients in the water column in a warm and hyper-saline oligotrophic environment.

2. Methodology

2.1. Sampling and oceanographic data

A bottom-tethered mooring has been deployed continuously since January 2014 near Station A, northern GOA (29°28'00.0"N, 34°55'45.0"E ~605 m water depth) (Torfstein et al., 2020). Five KC Denmark cylinder sediment traps were mounted vertically and located at depths of 120 m, 220 m, 350 m, 450 m, and 570 m below the surface. The trap samples were collected at a monthly resolution. Furthermore, PF samples from the sediment interface were collected using a box core ('core top'). Further detailed description of the mooring, sampling, sample processing, and trapping efficiencies can be found in Chernihovsky et al. (2018) and Torfstein et al. (2020). Here, we report the findings derived from the PF tests collected between June 2014 and June 2015. Water column physical and chemical parameters are routinely collected at Station A by the Israel National Monitoring Program (NMP, Shaked & Genin, 2016). This includes sea surface and water column temperature (°C), salinity, oxygen concentration (µmol/l), alkalinity (meq/kg), *p*H, and chlorophyll-a concentration (µg/l). Mixed layer depth (MLD) was defined as the shallowest depth where the TEOS-10 potential density anomaly (σ_0), computed with gsw from Practical Salinity and in-situ temperature with pressure from depth at Station A, exceeded a near-surface reference by $\Delta\sigma_0 = 0.03$ kg m^{-3}; the reference density was the median σ_0 within 0–10 m (or the shallowest 10 m available when the surface was not sampled). Temperature, salinity, and *p*H within the mixed layer were then calculated as thickness-weighted means by linearly interpolating each profile onto a 0.5 m grid and averaging from the surface to the MLD.

159 2.2. Species classification and preparation for LA-ICP-MS
160
161 We examined the shell chemical properties of two flux dominating PF species *T. clarkei*
162 and *G. ruber albus* (i.e., sensu stricto, white). For *T. clarkei* we examined two morphotypes:
163 'big' and 'encrusted'. Identification and nomenclature of the PF taxa followed Schiebel &
164 Hemleben (2017), Morard et al. (2019), and Brummer & Kucera (2022). Three individuals
165 were picked from each sediment trap depth during each month between June 2014 and June
166 2015. Preliminary preparation and cleaning steps are detailed by Chernihovsky et al. (2018).
167 Reductive and oxidative cleaning had been avoided to retain original signals related to the
168 different encrustation processes and preserve all calcite layers added to the shell during
169 ontogeny (Schiebel & Hemleben, 2017; Jochum et al., 2019). Specifically, the shell of *T.*
170 *clarkei* is prone to loss of material during reductive and oxidative treatment as it has very thin
171 chamber walls (ranging between 1.9 and 3.6 μm; Levy et al., 2023). Single chamber
172 measurements were performed to assess inter chamber variability (ICV), on individual shells
173 (individual foraminifer analysis; IFA) using Laser Ablation Inductively Coupled Plasma Mass
174 Spectrometry (LA-ICP-MS). We measured 156 specimens in total and 615 chambers: 57
175 individuals (168 chambers) of *G. ruber albus*, 52 individuals (242 chambers) of *T. clarkei* 'big'
176 and 48 individuals (204 chambers) of *T. clarkei* 'encrusted'. Samples were glued to glass slides
177 using a methyl-hydroxy-propyl-cellulose (MHPC 1:100), positioned with the umbilical side
178 up.
179
180 2.3. LA-ICP-MS and data processing
181 Analyses of the calcium-normalized elements for B, Na, Mg, Al, Ti, Mn, Fe, Co, Sr, Ba,
182 Nd, Pb, Th, and U were conducted using a 200 nm wavelength NWR femtosecond (fs) LASER
183 system from ESI, combined with a sector-field Thermo Element-2 ICP mass spectrometer
184 (Jochum et al., 2014). Measurements were performed using a 15 Hz pulse repetition rate (PRR),
185 at low fluence (0.1–0.6 J/cm^2), and 18 seconds dwelling time. A 30 μm diameter spot size was
186 selected, as it is the maximum diameter for analysis fitting in a single chamber of the small *T.*
187 *clarkei*. The microanalytical synthetic reference material MACS-3 for carbonate, NIST-612,
188 and NIST-610 were used for calibration. NIST-612 was used for the tuning of the ICP-MS
189 (Jochum et al., 2019). The average element-to-calcium ratio from the spot derived LA-ICP-MS
190 count data was calculated from count data immediately after the start of the ablation peak apex
191 until the point identified as the termination of calcite based on the Mg/Ca profile. This time

interval represents the stable internal material of the shell; excluding the noisy beginnings and ends of the ablation event. For *G. ruber* the mean ablation time length used for calculation was 4.9±2.3 secs, while for the smaller and thinner *T. clarkei* it was 2.6±1.5 secs and 2.4±1.4 secs, for 'big' and 'encrusted' types, respectively.

The measurement precision (1 relative standard deviation in percent; 1 RSD) yield uncertainties for references materials between ~ 5-17 % for the calcium-normalized elements (Supplementary table S1). Single spot measurements were made on each chamber of the individual shells. Chambers are labelled F0 (final chamber), F-1 (final minus one), F-2, and so on, for the penultimate, antepenultimate, and further chambers, respectively. We calculated averages and standard deviations of element/Ca of single individuals (calculated from all single chamber element/Ca in one shell) and relative standard errors of element/Ca of pooled measurements for a specific morphotype.

2.4 Statistical Analysis

We used redundancy analysis (RDA) to quantify how variation in shell element/Ca responses relates to environmental conditions (MLD, T, S, and *p*H). For each species, we assembled two time-aligned matrices by date: (i) a multivariate response matrix containing the element/Ca values at each sampled depth (120, 220, 340, 450, 570 m) plus the overall total, and (ii) an environmental matrix containing environmental predictors. RDA was fit using the vegan package in R (function rda), which is equivalent to multivariate multiple regression followed by PCA of the fitted values. Biplots were produced with arrows show the direction of increasing predictor values and their relative importance, and response points (depths/TOTAL) project positively or negatively onto each arrow according to their alignment, with the proportions of constrained variance carried by the first RDA axes (labels shown on the biplot axes). As a measure of specimen inter-chamber variability (ICV), the standard deviation (SD) was calculated for each individual. We calculated Spearman rank correlation matrices in R for each species across element/Ca and SD, together with environmental parameters, with the spearman correlation coefficients visualised as heatmaps (associated p-values reported in supplementary table's S2 and S3, respectively).

3. Results:

222 3.1. Shell-bound element/Ca time series trends in *G. ruber albus* and *T. clarkei* shells
223 Single chamber Mg/Ca over water column depths in *G. ruber albus* range between 2.01
224 mmol/mol (340 m; June 2015) and 18.49 mmol/mol (340 m; July-August 2014), with
225 lower/higher values during winter/summer months, respectively (Figs. 3b-3f). A unique
226 observation is an increase in Mg/Ca seen during spring (March-April), i.e., months with
227 maximum surface water column mixing, at some water depths (220 m, 340 m, 450 m; Figs. 3c-
228 3e). Accompanied with the Mg/Ca increase is a clear increase in ICV as evident by the
229 divergence of chamber values. The SD of *G. ruber albus* ranges between 0.14 in February 2015
230 at 450 m water depth and 7.27 during April 2015 at 120 m water depth. Generally, it appears
231 that Mg/Ca is lower in F0 chambers (orange dotted line) compared to preceding chambers,
232 especially during months with very shallow MLD (3a-3g). Mg/Ca in *T. clarkei* 'big' range
233 between 4.00 mmol/mol (340 m; June 2015) and 77.02 mmol/mol (220 m; March 2015) and
234 between 4.06 mmol/mol (570 m; December 2014) and 51.22 mmol/mol (120 m; April 2015)
235 in *T. clarkei* 'encrusted', respectively. For both *T. clarkei* 'big' and *T. clarkei* 'encrusted' there
236 are high excursions in all chambers during months of water column mixing while MLD is
237 deepest (circa April; 3j-3w). The SD ranges between 0.43 and 25.38 (120 m; September 2014
238 and, 220 m; April 2015 respectively) for *T. clarkei* 'big' and for *T. clarkei* 'encrusted' is up to
239 18.52 (340 m; March 2015).
240

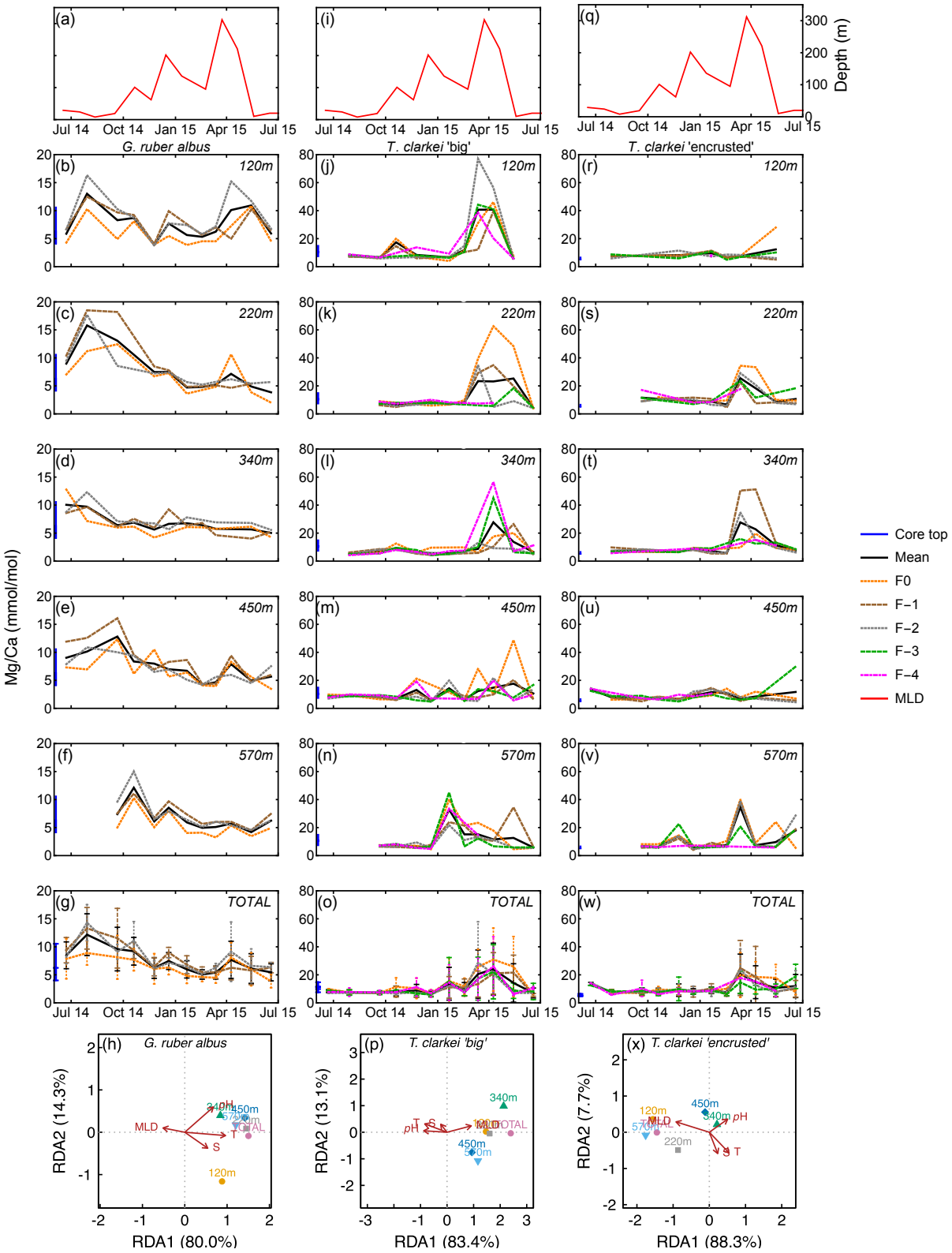

Figure 3: Time series of Mg/Ca values measured from the shells of *G. ruber albus* (b-f), *T. clarkei* 'big' (j-n) and *T. clarkei* 'encrusted' (r-v), derived from sediment traps located at different water depths (120-570 m). Mg/Ca of core top are marked by a blue bar along the left y-axes. Top panels a, i, and q show the depth (meters below surface layer) of the mixed layer

depth (MLD). Panels g, o, and w represent the average values of all depths for each chamber for each species. Panels h, p and x show the redundancy analysis (RDA) per species for each water depth with MLD depth, temperature, salinity and *p*H as explanatory variables.

The *G. ruber albus* RDA analysis of Mg/Ca show that most water depth samples, except for the 120 m are clustered together and align with temperature and MLD, positive and negative respectively. *Turborotalita clarkei* 'big' exhibits a contrasting image compared to *G. ruber albus* and positively correlates with MLD while negatively correlating with temperature, salinity, *p*H. All three morpho-species show a distinct dominance of RDA1 explaining >80% of the variance (Figs. 3h, 3p and 3x).

Sr/Ca in *G. ruber albus* range between 1.25 mmol/mol (570 m; January 2015) and 2.27 mmol/mol (340 m; November 2014) (Figs. 4b-4f). The SD in *G. ruber albus* ranges reaches up to 0.48 (220 m; November 2014). Single chamber Sr/Ca in *T. clarkei* 'big' range between 0.94 mmol/mol (340 m; January 2015) and 2.76 mmol/mol (220 m; April 2015) and for *T. clarkei* 'encrusted' between 0.54 mmol/mol (340 m; April 2015) and 2.92 mmol/mol (570 m; June 2015), respectively (Figs. 4j-4n, and 4r-4v). *Turborotalita clarkei* 'big' and *T. clarkei* 'encrusted' display more ICV than *G. ruber albus*, with peaking Sr/Ca in numerous chambers around April 2015 (Figs. 4j-4w). During the spring months of 2015, Sr/Ca values range between 1.45-2.04 mmol/mol in *G. ruber albus*, 1.32-2.76 mmol/mol in *T. clarkei* 'big' and 0.54-2.27 mmol/mol in *T. clarkei* 'encrusted', respectively (Fig. 4; Fig. S1). Additionally, the SD of *T. clarkei* 'big' is the highest at 0.43 in March 2015 at 120 m water depth, and lowest at 0.02 in June-July 2014, at 340 m water depth. For *T. clarkei* 'encrusted' SD reaches 0.7 (220 m; April 2015). While the RDA analysis of *T. clarkei* 'big' show a high RDA1 dominance (91.6%), the RDA1 of *G. ruber albus* and *T. clarkei* 'encrusted' are lower (75.9% and 67.1% respectively). In both *G. ruber albus* and *T. clarkei* 'big' the environmental factors (*p*H, salinity and temperature) point together and opposite to MLD, while in *T. clarkei* 'encrusted' salinity and MLD are more closely related.

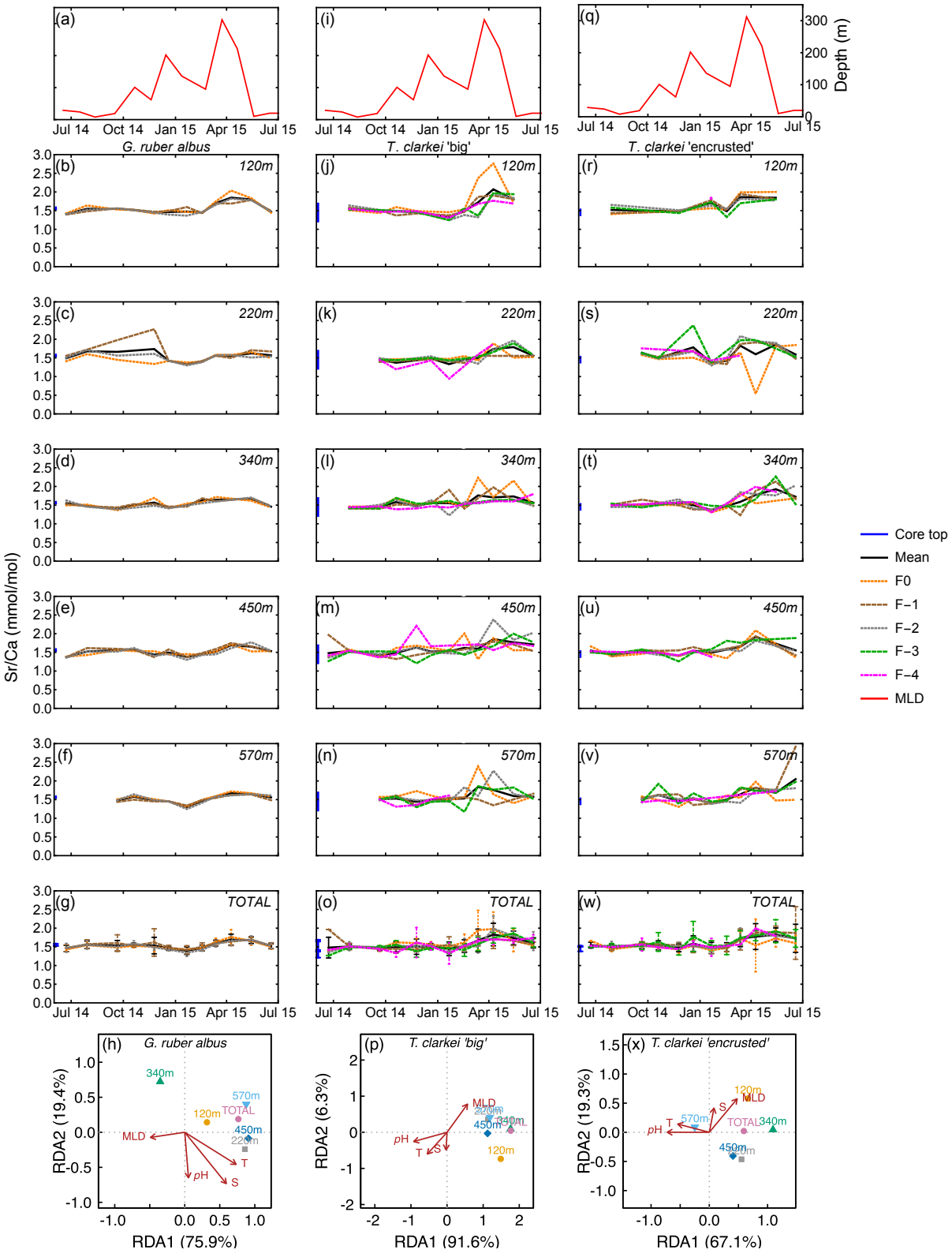

Figure 4: Time series of Sr/Ca values measured from the shells of *G. ruber albus* (b-f), *T. clarkei* 'big' (j-n) and *T. clarkei* 'encrusted' (r-v), derived from sediment traps located at different water depths (120-570 m). Sr/Ca of core top are marked by a blue bar along the left y-axes. Top panels a, i, and q show the depth (meters below surface layer) of the mixed layer

depth (MLD). Panels g, o, and w represent the average values of all depths for each chamber for each species. Panels h, p and x show the redundancy analysis (RDA) per species for each water depth with MLD depth, temperature, salinity and *p*H as explanatory variables.

B/Ca values range between 0.03 mmol/mol (570 m; January 2015) to 0.35 mmol/mol (120 m; June 2015) in *G. ruber albus*, with higher values during summer and spring and lower values during the winter (Figs. 5b to 5f). B/Ca measured in the final chamber, F0, are systematically lower compared to F-1 and F-2 values. Unlike most other element ratios, B/Ca values in both phenotypes of *T. clarkei* are similar to the range measured in *G. ruber albus*. In both *T. clarkei* phenotypes, lower B/Ca values were measured during the winter months, most prominently in January. The B/Ca values of *T. clarkei* 'big' range between 0.01 mmol/mol to 0.53 mmol/mol with some higher values during spring (Figs. 5k to 5n). B/Ca values in *T. clarkei* 'encrusted' range between 0.01 mmol/mol to 0.47 mmol/mol (Figs. 5r to 5v). Generally, B/Ca ICV is higher in *T. clarkei* than *G. ruber albus*, especially during spring (Figs. 5g, 5o, and 5w). The SD of *G. ruber albus* is highest at 0.086 during May 2015, at 120 m, and for *T. clarkei* 'big' and *T. clarkei* 'encrusted' the SD is 0.164 (450 m; June-July 2014) and 0.19 (120 m; May 2015) respectively. RDA analysis on B/Ca reveal a distinct RDA1 dominance in both *T. clarkei* 'big' and *T. clarkei* 'encrusted' (93.6% and 95.8%, respectively) compared to only 53.8% *in G. ruber albus*. In both *T. clarkei* phenotypes, the sediment trap data cluster together, showing a positive correlation with MLD and negative correlations with temperature, salinity, and *p*H. In contrast, *G. ruber albus* exhibits a more scattered distribution across water depths, with the 120 m and total samples showing a stronger alignment with MLD.

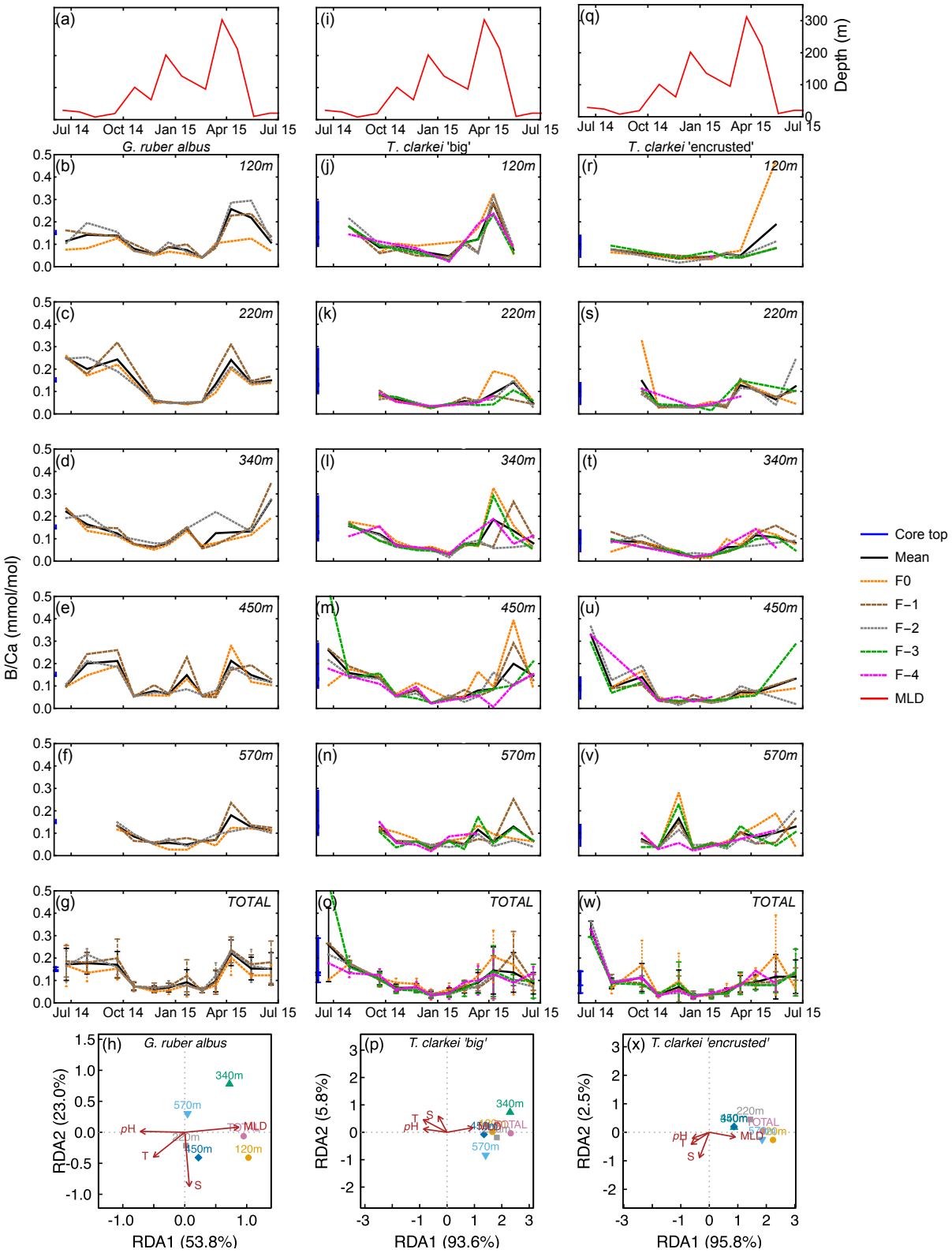

Figure 5: Time series of B/Ca values measured from the shells of *G. ruber albus* (b-f), *T. clarkei* 'big' (j-n) and *T. clarkei* 'encrusted' (r-v), derived from sediment traps located at different water depths (120-570 m). B/Ca of core top are marked by a blue bar along the left y-axes. Top panels a, i, and q show the depth (meters below surface layer) of the mixed layer depth (MLD).

Panels g, o, and w represent the average values of all depths for each chamber for each species. Panels h, p and x show the redundancy analysis (RDA) per species for each water depth with MLD depth, temperature, salinity and *p*H as explanatory variables.

Na/Ca in *G. ruber albus* ranges between 6.60 mmol/mol (220 m; June-July 2014) to 64.14 mmol/mol (220 m; April 2015) with a median value of 10.43 mmol/mol (Fig. 6; Fig. S1). The SD of Na/Ca ranges between 0.06 (570 m; February 2015) to 34.37 (120 m; April 2015). Na/Ca in *T. clarkei* 'big' ranges from 6.23 mmol/mol (570 m; September 2014) to 426.54 mmol/mol (220 m; March 2015) with a median value of 12.33 mmol/mol and SD range between 0.44 (570 m; September 2014) to 106.33 (120 m; March 2015). Na/Ca in *T. clarkei* 'encrusted' ranges between 5.43 mmol/mol (570 m; September 2014) to 176.91 mmol/mol (570 m; March 2015) with a median value of 12.41 mmol/mol and SD reaches up to 64.64 (340 m; March 2015). *Globigerinoides ruber albus* has a low ICV during spring, while *T. clarkei* 'big' and 'encrusted' phenotypes display higher ICV during the same time interval. All morphotypes include significant excursions in Na/Ca with high values in *G. ruber albus* during January and April at 220m (Fig. 6c), and high Na/Ca in both *T. clarkei* phenotypes at multiple depths and seasons (Figs. 6i-6m and 6p-6t). In particular, *T. clarkei* phenotypes show significant Na/Ca excursions during March-April and ICV (Figs. 6i-6t). RDA analysis on *T. clarkei* 'big' show, like B/Ca, a clustering of sediment trap data aligned with MLD and negatively correlated to *p*H, salinity and temperature positioned on the RDA1 axis (85.3%). The sediment trap data of *T. clarkei* 'encrusted' show two distinct groups: 120 m, 220 m, 570 m and 'Total' together with MLD and the 350 m and the 450 m groups in the middle between MLD and *p*H, salinity and temperature, albeit slightly negative on the RDA2 axis (9.0%), while the explanatory parameters are positive on RDA2. The *G. ruber albus* Na/Ca displays a similar distribution to B/Ca however, the environmental parameters are aligned differently: MLD negative on RDA1 axis (62.3%) and positive on RDA2 axis (28.1%); and, temperature, salinity and *p*H negative on RDA2 axis and positioned more to the center of RDA1.

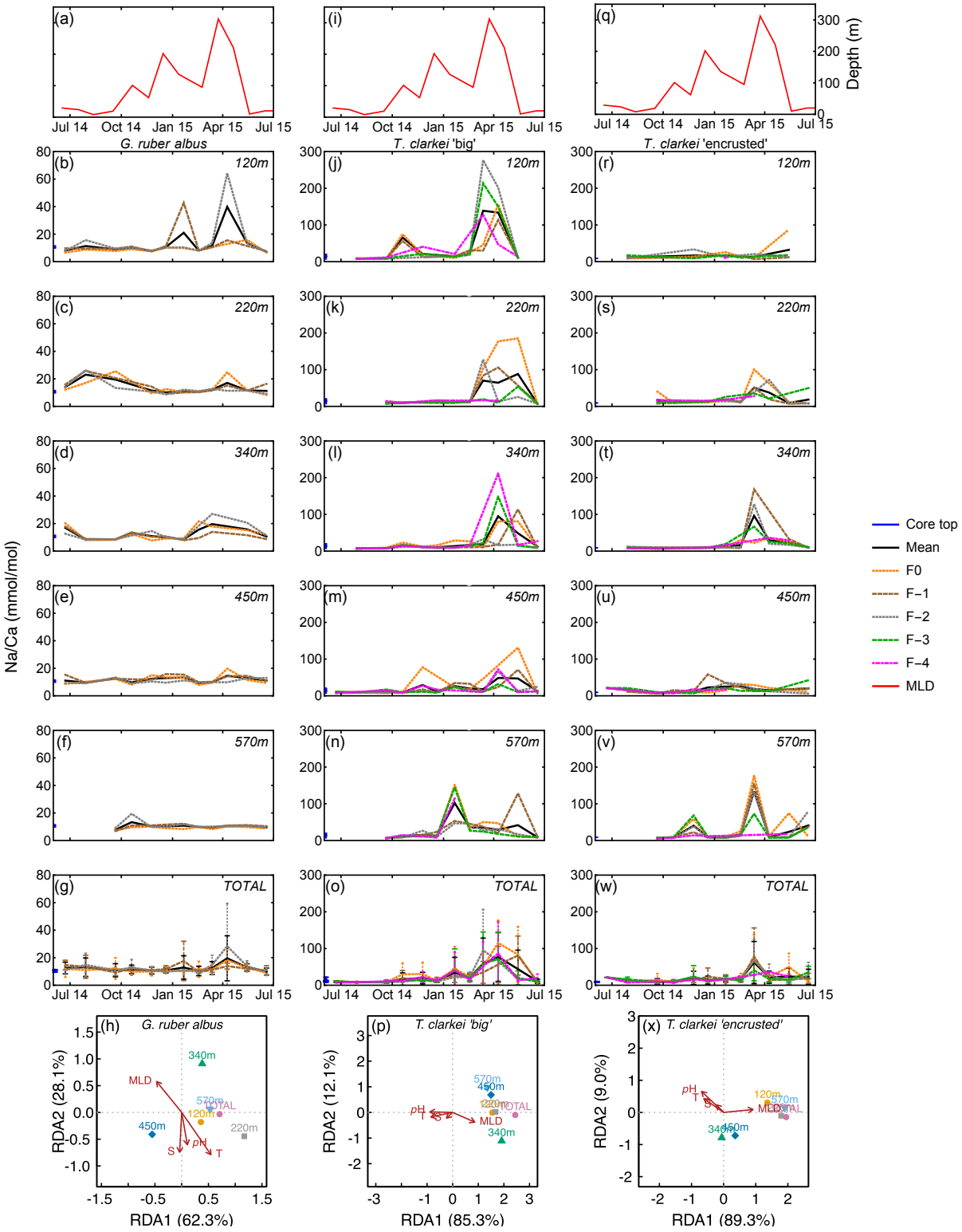

Figure 6: Time series of Na/Ca values measured from the shells of *G. ruber albus* (b-f), *T. clarkei* 'big' (j-n) and *T. clarkei* 'encrusted' (r-v), derived from sediment traps located at different water depths (120-570 m). Na/Ca of core top are marked by a blue bar along the left y-axes. Top panels a, i, and q show the depth (meters below surface layer) of the mixed layer depth (MLD). Panels g, o, and w represent the average values of all depths for each chamber

for each species. Panels h, p and x show the redundancy analysis (RDA) per species for each water depth with MLD depth, temperature, salinity and *p*H as explanatory variables.

Ba/Ca in *G. ruber albus* ranges from 0.73 µmol/mol (120 m; November 2014) to 36.81 µmol/mol (340 m; June 2015). Ba/Ca in *T. clarkei* 'big' ranges from 0.39 µmol/mol (120 m; June 2015) to 246.54 µmol/mol (450 m; March 2015). Ba/Ca in *T. clarkei* 'encrusted' ranges from 0 µmol/mol (April 2015) to 171.41 µmol/mol (340 m; March 2015) (Fig. 7; Fig. S1). The three morphotypes display varied ICV, although *T. clarkei* shows more prominent ICV during spring months with SD values of 42.06 (340 m; April 2015, 'encrusted') and 98.98 (450 m; March 2015, 'big) (Figs. 7i-7t and supplementary table S4) than *G. ruber albus* with SD values of 19.14 (220 m; June-July 2014) (Figs. 7b-7f). Furthermore, RDA analyses exhibit for both *T. clarkei* phenotypes, a clear RDA1 dominance with 93.6% and 95.8% for 'big' and 'encrusted' respectively. Additionally, for both types, sediment trap data is clustered with positive correlation to MLD and negative to temperature, salinity and *p*H. For *G. ruber albus*, RDA1 value is 53.8% and RDA2 is 23.0%. The sediment traps data are scattered and while the environmental parameters temperature and salinity point together negatively on the RDA2 axis, MLD and *p*H are positioned on opposite directions on the RDA1 axis (positive and negative respectively).

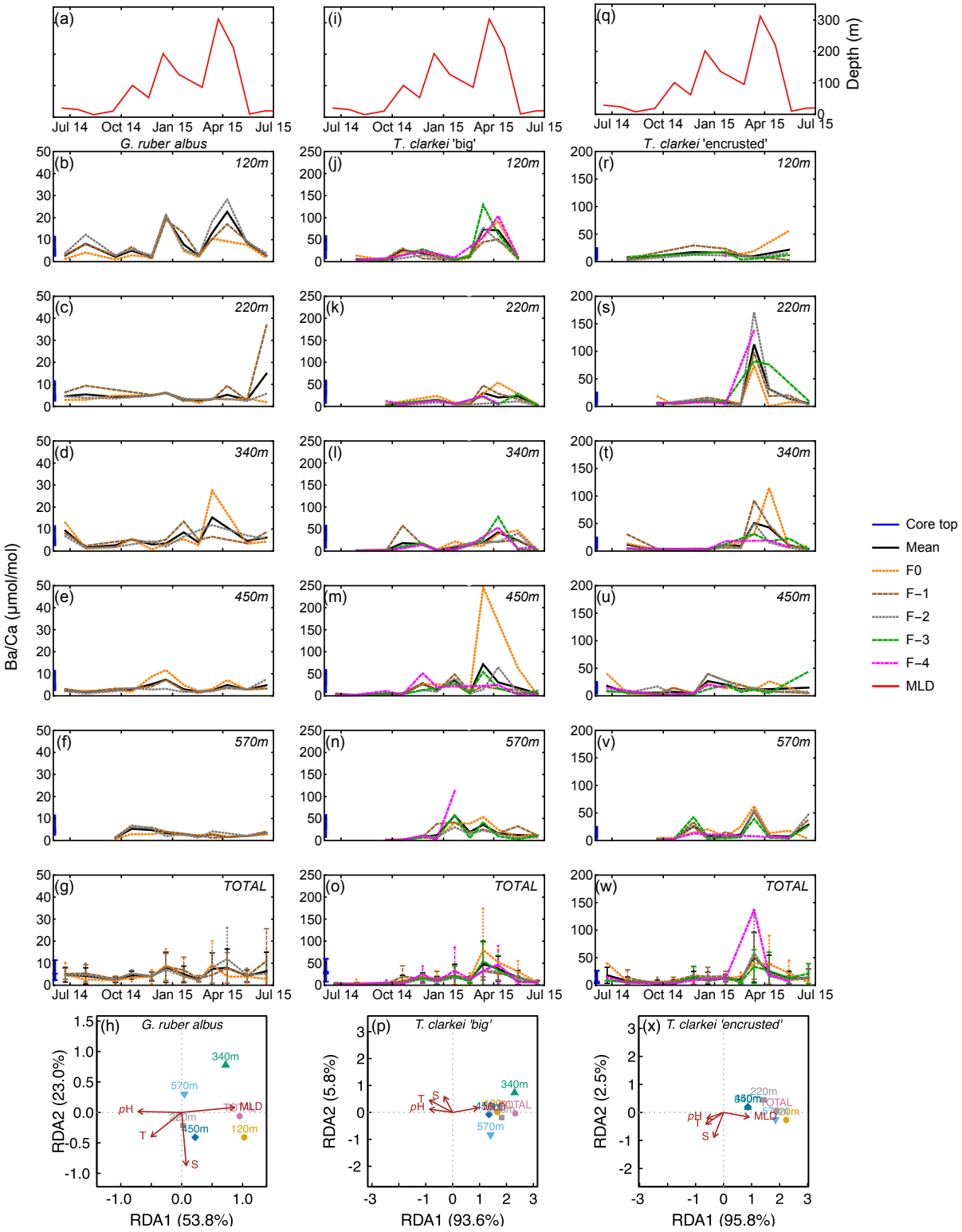

Figure 7: Time series of Ba/Ca values measured from the shells of *G. ruber albus* (b-f), *T. clarkei* 'big' (j-n) and *T. clarkei* 'encrusted' (r-v), derived from sediment traps located at different water depths (120-570 m). Ba/Ca of core top are marked by a blue bar along the left y-axes. Top panels a, i, and q show the depth (meters below surface layer) of the mixed layer depth (MLD). Panels g, o, and w represent the average values of all depths for each chamber

for each species. Panels h, p and x show the redundancy analysis (RDA) per species for each water depth with MLD depth, temperature, salinity and *p*H as explanatory variables.

3.2. Depth-averaged values of element/Ca measured in *G. ruber albus* and *T. clarkei* shells using LA-ICP-MS

Generally, the means of Mg/Ca, Sr/Ca, B/Ca, Na/Ca and Ba/Ca in *G. ruber albus* indicate that the composition of tests, from most water depths is similar to that of core-top samples (Figs. 8a-8d, 8j). In contrast, Al/Ca, Ti/Ca, Mn/Ca, Fe/Ca, Nd/Ca, Th/Ca, and U/Ca (Figs. 8e-8i, 8k, 8m, 8n) in the tests from sediment interface were higher than in the water column, and lower in case of Co/Ca and Pb/Ca (Figs. 8i, 8l).

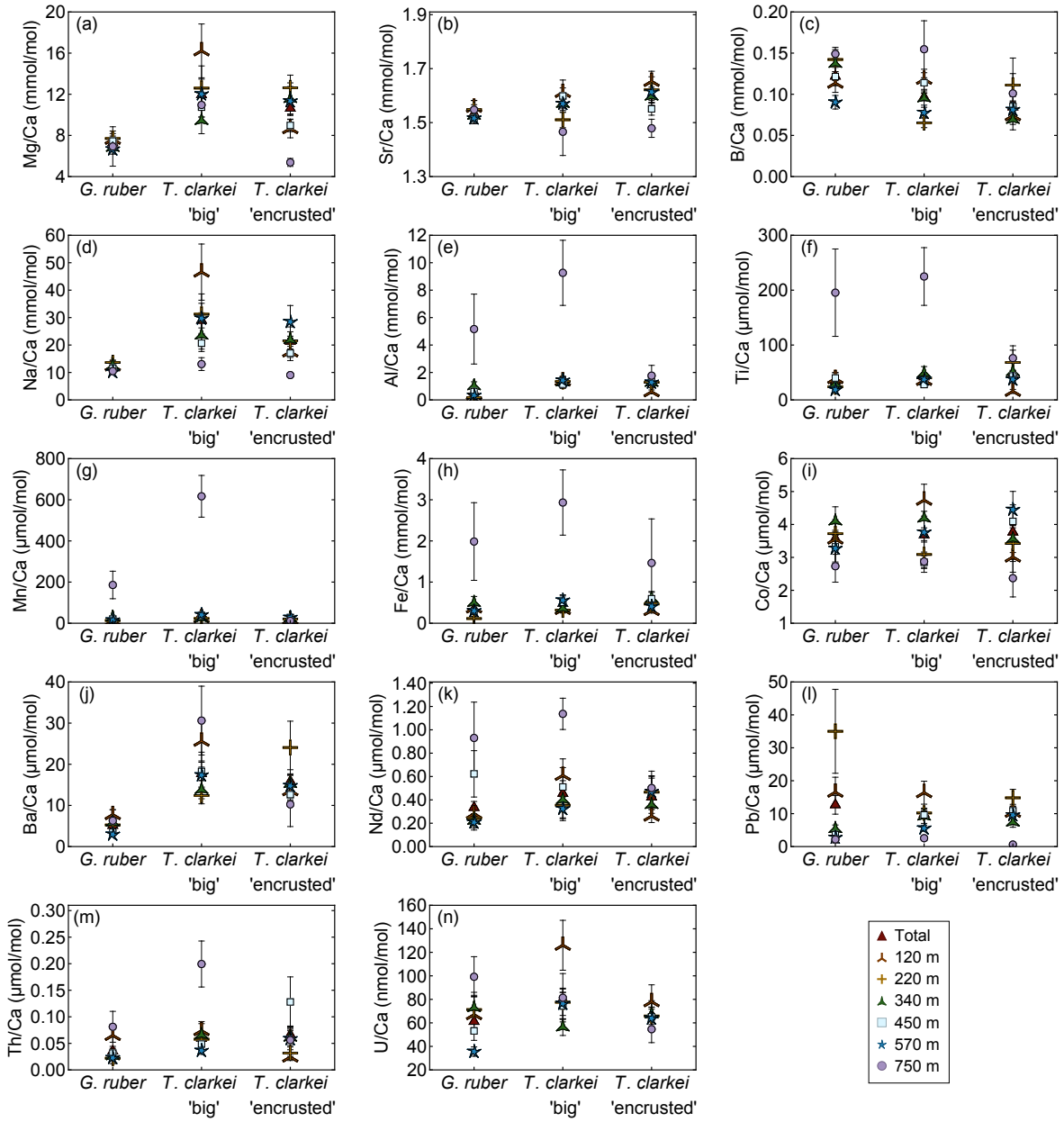

Figure 8: Pooled mean values of the calcium-normalized element ratios of *G. ruber albus*, *T. clarkei* 'big' and *T. clarkei* 'encrusted' shells, derived from sediment traps located at different water depths (120 m to 570 m) and a core top sample (750 m) from the Gulf of Aqaba. Error bars represent 1 sigma relative standard error ($SD/\sqrt{n}$).

Furthermore, *T. clarkei* tends to demonstrate higher values and higher variability compared to *G. ruber albus* (e.g., Mg/Ca, Na/Ca, Ba/Ca, Nd/Ca). Compared to the core-top samples, *T. clarkei* from the water column also exhibit relative enrichment in Al/Ca, Ti/Ca, Mn/Ca, Fe/Ca, Nd/Ca, B/Ca, and Th/Ca (*T. clarkei* 'big'), and depletion in Co/Ca, Pb/Ca, Sr/Ca, and Mg/Ca (*T. clarkei* 'encrusted') (Fig. 8).

3.3. Relationships between element/Ca and environmental parameters

A Spearman correlation matrix was applied to assess the relationships of the element/Ca and environmental variables in the three analyzed PF phenotypes (Fig. 9; Tab. S2; Fig S12). The *T. clarkei* types exhibit similar pattern of relationships, with minor differences mainly in correlation strength (Fig. 9a, 9b). In general, *T. clarkei* shows more significant relationships than *G. ruber albus*, while, *G. ruber albus*, display different relationships to those of the two *T. clarkei* types. In *T. clarkei,* Mg/Ca displays relatively strong relationships with Na/Ca, Ba/Ca, and Al/Ca (Fig. 9b, 9c). Sr/Ca, B/Ca, Co/Ca and Nd/Ca do not display significant relationships to other elements in *G. ruber albus* as well as in *T. clarkei* 'big' and *T. clarkei* 'encrusted'.

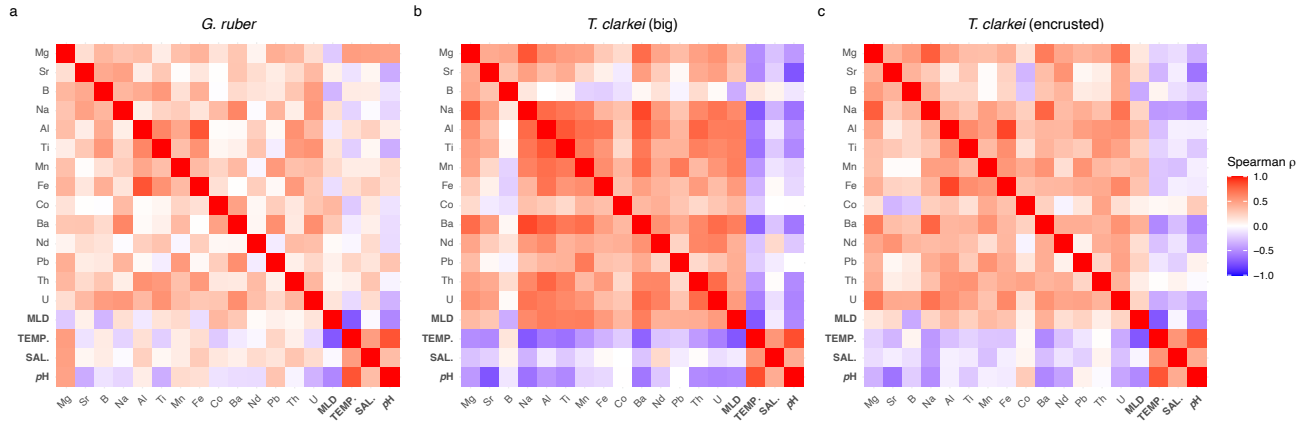

Figure 9: Spearman correlation Matrix of element-Ca means in *G. ruber albus* (a), *T. clarkei* "big" (b) and, *T. clarkei* "encrusted" (c) and environmental variables.

For both *T. clarkei* 'big' and *T. clarkei* 'encrusted', Na/Ca significantly correlates with Al/Ca, Mn/Ca, and Ba/Ca, the later showing the strongest relationships in *T. clarkei* 'big' (r = 0.82, Fig. 9b; Tab. S2). Relationships between Al/Ca, Ti/Ca, Mn/Ca, Fe/Ca, Ba/Ca and Th/Ca are generally stronger in *T. clarkei 'big'* than in *T. clarkei 'encrusted'*, except for Al/Ca and Fe/Ca, which are stronger related in *T. clarkei 'encrusted'* (r = 0.85; Tab. S2) than in *T. clarkei 'big'* (r = 0.74; Tab. S2). Unlike *G. ruber albus*, the U/Ca in *T. clarkei* exhibit relatively strong relationships with Ba/Ca, Na/Ca and Al/Ca (in *T. clarkei* 'big') and Mg/Ca (in *T. clarkei* 'encrusted', Fig. 9c) while in *G. ruber albus*, U/Ca is poorly related to the other elements (Fig. 9a). Mg/Ca of *G. ruber albus*, has a positive correlation with temperature, salinity, and *p*H, and a negative correlation with MLD; other element/Ca in *G. ruber* albus do not exhibit significant correlations with these environmental variables (Fig. 9a). By contrast, in *T. clarkei* ('big' and 'encrusted'), element/Ca show strong correlations with MLD but not with temperature, salinity, or *p*H (Figs. 9b, 9c). In the *T. clarkei* 'big' morphotype, SD (ICV) shows strong correlations between multiple element/Ca and with MLD. On the other hand, in *T. clarkei* 'encrusted' and *G. ruber albus*, correlations are weaker and/or inconsistent across variables, and no uniform pattern emerges.

4. Interpretation

4.1 Inter chamber variability (ICV)

Shell-bound element/Ca display varying trends across different chambers depending on the specific element ratios, and varying over water depth and time (Figs. 3-7). In most element/Ca ICV is higher during water column mixing months (March-May; e.g., Al/Ca, B/Ca, Ba/Ca, Co/Ca, Fe/Ca, Mg/Ca) in all water depth horizons for *T. clarkei* 'big' and *T. clarkei* 'encrusted', while for *G. ruber albus* it increases in the two upper water depth horizons (i.e., 120 m and 220 m). Elevated element/Ca values and high ICV may reflect the changes in the water properties like the temperature, salinity, *p*H and nutrient availability derived from the mixing of the water column (Fig. S12, Figs 3-7 panels h, p, and x). For some element/Ca ratios (e.g., Na/Ca, Fig. 6/panels g, o, and w; Ba/Ca, Fig. 7/panels g, o, and w) ICV varies with depth and shows seasonal differences (i.e., less variation with depth during water column stratification and more variation with depth during water column mixing), whereas for others (e.g., B/Ca, Fig. 5/panels g, o, and w; Sr/Ca, Fig. 4/panels g, o, and w) it remains relatively constant with depth. In the *T. clarkei* 'big' morphotype, ICV shows strong correlations across most element/Ca and with MLD, indicating that increases in ICV reflects a common driver, most likely the mixed-layer depth (Fig. S12).

Typically, most PF reproduction-cycles span about a month with individual chambers forming within several hours (Bé et al., 1977), while the time interval between chamber formation can range from hours to weeks (Schiebel & Hemleben, 2017, and references therein). Setting aside the March-May time-interval where PF shells show exceptionally high ICV, *G. ruber albus* generally exhibits lower values (e.g., Mg/Ca, B/Ca), and less ICV compared (e.g., Mg/Ca SD=1.67) to *T. clarkei* 'big' and 'encrusted' (e.g., Mg/Ca SD=5.24 for 'big' type and Mg/Ca SD=3.55 for 'encrusted' type). The residence of *G. ruber albus* in the relatively homogenous and narrow living environment in the surface mixed layer (Schiebel & Hemleben, 2017; Thirumalai et al., 2014; and others), could explain relatively lower ICV. In contrast, *T. clarkei* dwell in the dynamic region near/under the thermocline (Schiebel & Hemleben, 2017; Levy et al., 2023) over a wider dwelling depth horizon, and may experience more heterogeneous environmental conditions which may result in higher ICV.

The secondary crust observed on *T. clarkei* 'encrusted' morphotypes, which covers all chambers of the tests analyzed here, does not significantly alter element/Ca values when compared to *T. clarkei* 'big', unlike the crust of *Neogloboquadrina dutertrei* (Jonkers et al., 2012). Nonetheless, the RDA (Figs. 3-7) and the Spearman correlation analyses (Fig. 9) of both *T. clarkei* types indicate that while *T. clarkei* 'big' show a positive correlation to MLD and a weaker or negative correlation to other environmental parameters (T, S and *p*H), the *T. clarkei* 'encrusted' type calcification mechanism is more complex and could be influenced by additional factors / environmental variables. Therefore, while both types are eligible for paleoceanography and paleoclimate reconstructions, the interpretation of their measurements might be different.

The ultimate chamber (F0) presents different systematics compared to the preceding chambers in both *T. clarkei* and *G. ruber albus* (Fig. S11). In *T. clarkei* (both 'big' and 'encrusted'), the F0 typically exhibits higher values of B/Ca, Na/Ca, Mg/Ca, and Al/Ca compared to the previous chambers. In contrast, *G. ruber albus* displays relatively lower values in F0 for the same ratios highlighting species-specific differences in chamber formation (Fig. S11). Interestingly, Sr/Ca does not follow the same pattern. In *T. clarkei* 'big' the Sr/Ca distribution mirrors the trends of other elements, while F0 in *G. ruber albus* and *T. clarkei* 'encrusted' shows an even distribution of Sr/Ca, likely reflecting the relatively constant Sr/Ca values in the water column during the lifespan of a single test. These observations in *G. ruber albus* are consistent with previous studies that measured Mg/Ca in individual chambers (Bolton et al., 2011; Davis et al., 2020; Fischer et al., 2024). The contrasting systematics of F0 leading to elevated ICV in the ultimate chamber compared to the previous chambers was previously

suggested to be associated with a chamber wall that is not fully calcified (Schiebel & Hemleben, 2017; Bolton et al., 2011; Fischer et al., 2024). Differences in F0 systematics between *T. clarkei* and *G. ruber albus* could be driven by species-specific calcification processes, though further research is needed to clarify this issue. Additionally, it is important to consider potential biases in small chambers such as F-4 in *T. clarkei* morpho-species, where methodological challenges (e.g., laser spots hitting sutures) may skew element/Ca measurements. Consequently, we conclude that the exclusion of F0 and F-4 may enhance the robustness of reconstructions of the marine environment in studies of downcore records.

4.2 Relationships of element ratios of the three PF morphotypes

The contrasting results of the correlation matrixes of the three morpho-species, suggests species-specific mechanisms while calcifying their shells. The Mg/Ca in *T. clarkei* which strongly correlates with Na/Ca, Ba/Ca, and Al/Ca (Fig. 9b, 9c), suggests more than one environmental process affects Mg/Ca in the tests as the other element/Ca are considered proxies to different environmental characteristics such as salinity, productivity, and terrigenous input (Chang et al., 2015; Mesa-Fernández et al., 2022; Beasley et al., 2021). This is also reinforced by the positive correlation to MLD and the negative correlation to temperature, salinity and *p*H (Fig. 9 and RDA panels in figs. 3-7). Additionally, Mg/Ca *in G. ruber albus* show a relative strong positive correlation to temperature, salinity and *p*H and a negative correlation to MLD (Fig. 9a and Figs. 3h, 3p and 3x). Similar to *G. ruber albus*, in the *T. clarkei* types Sr/Ca, B/Ca, Co/Ca and Nd/Ca display a much weaker relationship to other elements making them more suitable proxies for distinct and independent environmental properties.

In *G. ruber albus*, Mg/Ca, Sr/Ca and B/Ca show no significant relationships with other element ratios, indicating that independent processes likely govern their proxy systematics (Fig. 9c). Similarly, Co/Ca, Nd/Ca and U/Ca also do not correlate with other element/Ca. While Na/Ca and Ba/Ca exhibit some degree of correlation, as do Mn/Ca and Pb/Ca, the lithophilic elements, Al/Ca, Ti/Ca, which are considered proxies for terrigenous dust input (Chang et al., 2015; Mesa-Fernández et al., 2022; Beasley et al., 2021), as well as, Fe/Ca, and Th/Ca, all show a relative strong correlation. Their correlation implies they can be used together for reconstructing terrigenous input to the water column. Among the lithophilic elements, Th/Ca display a relatively weaker relationship, suggesting a potential effect of additional processes such as scavenging (Anderson et al., 1983; Francois et al., 2004; Costa et al., 2020).

4.3 Mg/Ca as a proxy for sea surface temperature

Shell-bound Mg/Ca of calcareous foraminifera have been extensively utilized as a paleo-thermometer (e.g., Nürnberg et al., 1996; Sadekov et al., 2009). Many of these Mg-temperature calibrations rely on whole-test or pooled-mean Mg/Ca values to reconstruct past sea surface temperatures (Spero et al., 2003; Ganssen et al., 2010; and others). Several studies have measured intra-test and inter-test Mg/Ca in an effort to produce Mg-temperature calibrations using single chamber measurements of *G. ruber* (Sadekov et al., 2008; Bolton et al., 2011; Davis et al., 2020; Levy et al., 2023; Fischer et al., 2024). Previous work on sediment trap-derived specimens of *T. clarkei* and *G. ruber albus* from the GOA indicated that *T. clarkei* is not suitable for temperature reconstructions, due to its presumed deep dwelling-depth below the thermocline together with its high sensitivity to water column mixing events. However, while *G. ruber albus* shows exceptionally high pooled mean Mg/Ca values in the GOA in comparison to other ocean regions, it also exhibits seasonal variations that indicate effective applicability as a paleothermometer (Levy et al., 2023). Due to the high seawater salinity of the GOA, a local calibration curve was proposed (Eq. 1; Levy et al., 2023).

$$\frac{\mathrm{Mg}}{\mathrm{Ca}} = 0.39(\pm 0.30) \cdot \mathrm{e}^{0.12(\pm 0.03)\mathrm{T}} \quad (1)$$

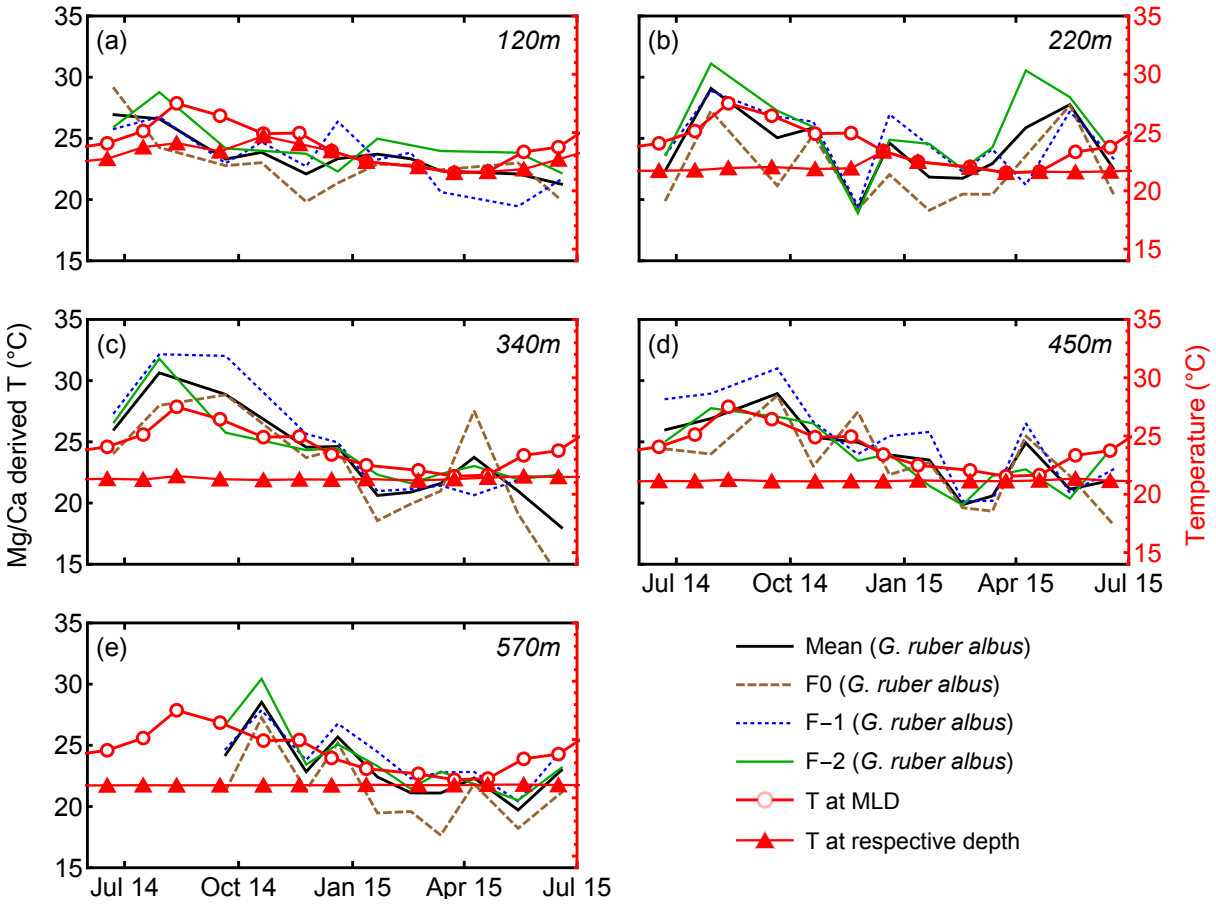

Figure 10: *G. ruber albus* Mg/Ca-derived temperatures versus measured temperatures (red). The calculated temperatures were derived from Eq. 1 for individual chambers. See also Levy et al. (2023).

Pooled mean values of Mg/Ca in *G. ruber albus* taken from all water column depths in the GOA reflect MLD temperatures (Fig. 10, Fig 9). Inter-chamber variability (ICV) has been shown to affect the local Mg/Ca temperature calibration (Eq. 1) of *G. ruber albus* (Levy et al., 2023; Fig. 10). Generally, Mg/Ca-derived temperatures from chambers F-1 and F-2 correspond closely with mixed layer depth (MLD) temperatures. However, beneath the photic zone, Mg/Ca of all three chambers F0, F-1, and F-2 of the *G. ruber albus* specimens exhibit poor fits with measured temperatures (Fig. 10). Given that *G. ruber albus* calcifies its shell in the photic zone (Schiebel and Hemleben, 2017), these findings support the use of Mg/Ca as a paleothermometer for the mixed layer (Nürnberg et al., 1996). Sadekov et al. (2009) measured F0-Mg/Ca in core top individuals of *G. ruber albus* from various latitudes and have reported an agreement with sea surface temperature. Hupp and Fehrenbacher (2024) measured intra-test variability in the polar and sub-polar species *Neogloboquadrina incompta*, *N. pachyderma*, and *Turborotalita quinqueloba* and have not reported any issues regarding the use of F0 for

temperature reconstruction. In the GOA however, the Mg/Ca-derived temperatures from chamber F0 calculate lower Mg/Ca temperatures of the MLD than chambers F-1 and F-2 (Fig. 10). Although Mg/Ca data from chambers F-1 and F-2 appear suitable for reconstructing temperatures and demonstrate agreement with MLD temperature trends, the high ICV in *G. ruber albus* is evidently too great to accurately reflect ambient temperatures using this calibration. Therefore, and based on these new observations, we suggest that optimal Mg/Ca-temperature calibration (Eq. 1) should be based on the pooled mean of the F-1 and F-2 chambers at all depths as the final chamber might lead to different results while reconstructing temperature.

4.4 B/Ca as a proxy for *p*H

B/Ca in some PF species has been suggested to be a proxy for *p*H (Yu et al., 2007; Allen et al., 2011). Comparing chamber B/Ca of both *G. ruber albus* and *T. clarkei* (both 'big' and 'encrusted') alongside *p*H at various water column depths in the GOA reveals contrasting results. While B/Ca in *G. ruber albus* exhibits seasonality (Fig. 5), with lower values during winter months, it does not appear to be consistent with the *p*H of respective water depth nor the MLD (Fig. 11). This inconsistency suggests that B/Ca in *G. ruber albus* from the GOA is not a reliable recorder of ambient water *p*H. Similarly, Henehan et al. (2015) and Naik & Naidu (2014) reported that B/Ca of open ocean core-top samples and down-core sediment samples do not display a *p*H relationship.

Alternatively, B/Ca in *G. ruber albus* may be sensitive to salinity and micro-environments produced by PF symbionts with *p*H levels which are distinct from the ambient water column. Culture experiments have shown that B/Ca is affected by salinity and increases with increasing salinity (Allen et al., 2012). However, only small salinity changes occur in the GOA (Fig. 1), which argue against a strong B/Ca-salinity relationship that would result in a B/Ca seasonal trend. It was suggested that photo-symbionts such as dinoflagellates in *G. ruber albus* create micro-environments with *p*H levels, which are distinct from ambient seawater, to accommodate for their photosynthetic activity, and indicate that B/Ca is more affected by *p*H in those micro-environments than the water column *p*H (Hönisch et al., 2021; Babila et al., 2014). An additional observation for the *G. ruber albus* B/Ca values is that they are relatively high in comparison to values from other studies. The relatively high salinity in the GOA (~41), combined with the photosymbiont activity in *G. ruber albus* may explain the elevated B/Ca values (Henehan et al., 2015; Hönisch et al., 2021; Babila et al., 2014).

In contrast to *G. ruber albus*, B/Ca in the photosymbiont barren *T. clarkei* may possibly record the changes in *p*H (Fig. 11) of seawater at its assumed ambient dwelling depth (i.e., 340 m-570 m), indicative of shifting between the deeper water column depth horizons where *p*H changes are evident. Based on the fluxes of *T. clarkei* (Chernihovsky et al., 2018; Fig. 2), the B/Ca of *T. clarkei* in the sediment record likely represent the *p*H beneath the thermocline and within the deep-water column horizons for specimens that lived from early winter through spring. In particular, *p*H at 340 m trends appear to follow the B/Ca trends of *T. clarkei* types. For B/Ca-*p*H calibrations utilizing the pooled mean of data from the chambers F-1, F-2, and F-3 may be used, while excluding the F0 and F-4 chambers where more ICV is visually apparent (Fig. 11).

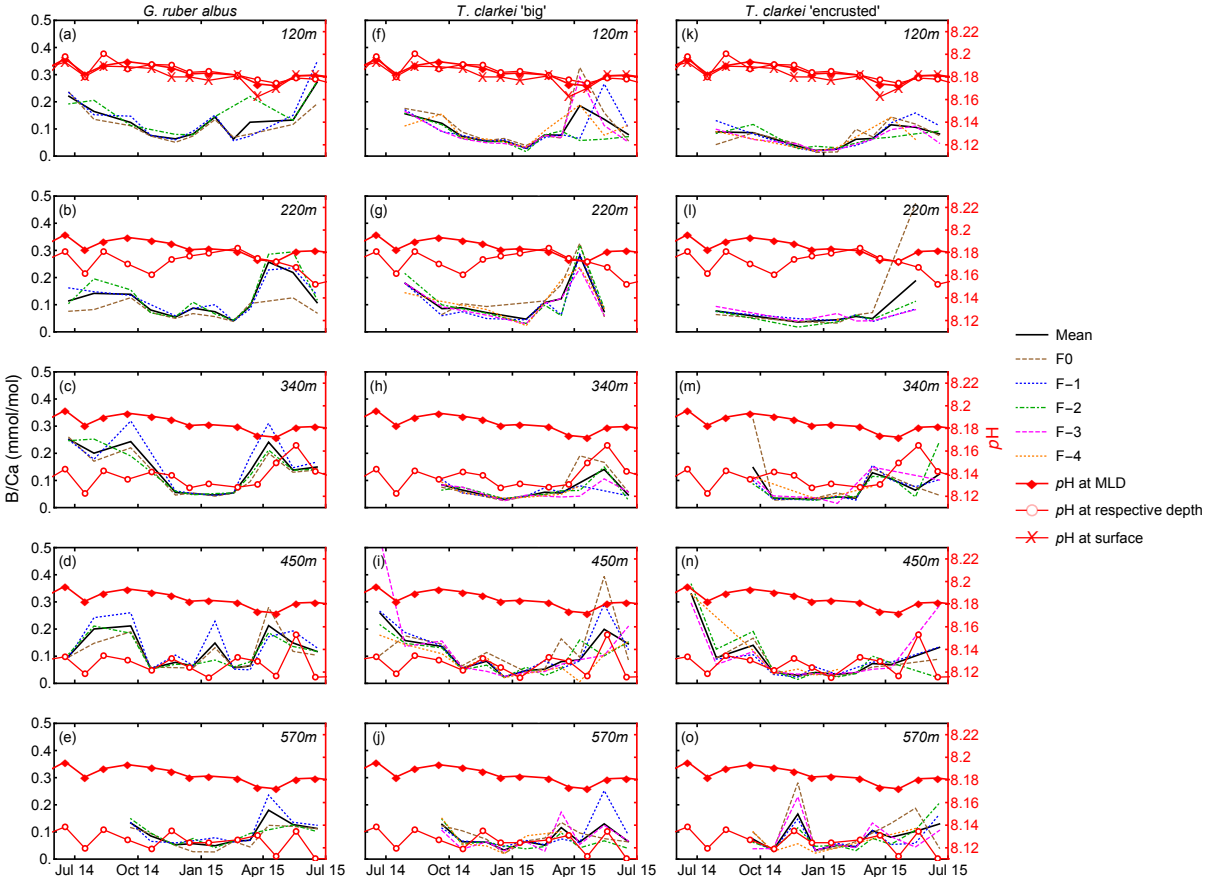

Figure 11: Single chamber B/Ca and in situ *p*H measured at MLD depth (empty red circles) and 120 m water depth for *G. ruber albus*, *T. clarkei* 'big' and *T. clarkei* 'encrusted'.

4.5 Na/Ca as a proxy for salinity and Ba/Ca as an indicator for productivity

Cultured individuals and samples from the surface Caribbean and the Gulf of Guinea of live *T. sacculifer* indicate that Na/Ca can be used as a proxy for salinity, without temperature dependence, however, a species-specific calibration might be required (Bertlich et al., 2018).

Despite the high variability of PF Na/Ca values in the GOA during water column mixing (Fig. 6), salinity remains high and relatively constant, ranging between 40.4-40.7. Consequently, a local Na/Ca-salinity calibration shows no significant relationship for any of the three PF morphotypes.

Na/Ca values in PF from the GOA are notably higher compared to other regions. Gray *et al.* (2023) explored the relationship between Na/Ca and salinity in *G. ruber albus* collected from sediment traps, plankton tows, culture samples, and core top samples, contributing to the ongoing discussions regarding the reliability of Na/Ca as a proxy for salinity in both planktic and benthic foraminifera (Allen et al., 2016; Geerken et al., 2018; Mezger et al., 2016, 2018; Gray et al., 2023, and references therein). They concluded that the measurement method (i.e., 'solution' ICP-MS vs. LA-ICP-MS) influences the values of Na/Ca and in turn the relationship with salinity, i.e., weak in solution-based compared to significant in laser ablation-based, at salinity over 36.

Comparing Na/Ca of *G. ruber albus* from the shallowest sediment trap (120 m) in the GOA with the Na/Ca of *G. ruber albus* plankton tows-samples from the GOA deployed and collected in January 2010 and October 2013 (Gray et al., 2023), both measured using LA-ICP-MS, generally reveals similar results, excluding the high-value excursions observed in some single chamber measurements (Fig. 6). *Turborotalita clarkei* in the GOA exhibits elevated Na/Ca values in both 'big' and 'encrusted' compared to *G. ruber albus*. Unlike *G. ruber albus*, there is relatively higher variability between water depths as well as significantly higher values in March, April, and May associated with water column mixing (Fig. 6). During these mixing events, nutrient-rich, high salinity (~40.7) water ascend upward. Therefore, the Na/Ca of *T. clarkei* may serve as a proxy for water column stability, i.e., stratification vs. mixing.

The Ba/Ca in the three morpho-species show a relatively strong correlation with Na/Ca (0.74 and 0.82 in *T. clarkei* 'big' and 'encrusted' respectively, and 0.54 in *G. ruber albus*, the second highest ratio and exceeded only by the 0.57 of Pb/Ca). Ba/Ca is presumably unaffected by temperature, salinity, and *p*H (Hönisch et al., 2011). In non-spinose species, Ba/Ca typically shows positive relationships with productivity and potentially can be used as an indicator of river run-off (Fritz-Endres et al., 2022; Hönisch et al., 2011; Weldeab et al., 2014). Although floods in the catchment area of the GOA are brief and occur only few times each year (Katz et al., 2015), significant Ba/Ca perturbations during water column mixing may reflect nutrient-rich water admixing to the surface water (Fig. 7).

5. Discussion:

621

622 5.1 Temporal and vertical dynamics of element/Ca in the GOA

623 Trace element incorporation into the calcium carbonate shells of planktic foraminifera during
624 calcification is controlled by environmental and ecological factors in the water column such as
625 temperature, salinity, *p*H, the carbonate system, dust and terrigenous inputs, as well as whether
626 a species harbor photosymbionts (Schiebel & Hemleben, 2017; and others). Shells of *G. ruber*
627 *albus*, *T. clarkei* 'big' and *T. clarkei* 'encrusted' from the GOA show species-specific behavior
628 and offer new insights into how these species respond to the vertical and temporal variations
629 in the water column. For most elements, the smaller *T. clarkei* specimens display higher trace
630 element ratios than the larger *G. ruber albus*, suggesting more efficient trace element
631 incorporation to the shell or implying that its habitat deeper in the water column has conditions
632 which result in higher trace element incorporation (Fig. 8). Some element ratios such as Mg/Ca,
633 Sr/Ca, B/Ca, Na/Ca (for *G. ruber albus*) and Ba/Ca for both *G. ruber albus* and *T. clarkei*
634 'encrusted', show overlap between specimens from the water column and from core-tops (Fig.
635 8), confirming the robustness of downcore-based records allowing to further consider these
636 element/Ca recorders of the water column as paleo-proxies.

637 While water depth likely influences element/Ca through variations in physical and
638 chemical conditions, the observed inter-chamber variability (ICV) and element/Ca differences
639 between species cannot be attributed to any single environmental parameter. Nonetheless,
640 elements such as Al/Ca, Ti/Ca, Mn/Ca, and Fe/Ca for all species, and Mg/Ca, Sr/Ca, Na/Ca,
641 and Ba/Ca for *G. ruber albus* alone, demonstrate consistent behavior across the water column,
642 suggesting that depth-related factors do not significantly alter calcification mechanisms. This
643 supports the use of pooled mean values for specimens over multiple sediment traps spread over
644 depths (Levy et al., 2023). Interestingly, most element/Ca peak during water column mixing in
645 March-April 2015 for all three morphotypes analyzed here, accompanied by larger ICV (Figs.
646 3-7). Mg/Ca in *G. ruber albus* and Sr/Ca in all three morpho-species show less pronounced
647 excursions, while other trace element ratios (e.g., Co/Ca, U/Ca) exhibit more variability and
648 more extreme values (Figs. S5 and S10). These observations can reflect: i) primary calcite
649 structure alterations driven by environmental shifts and life cycle changes, ii) secondary
650 mineralization (e.g., barite, Amorphous Calcium Carbonate, ACC) (Torres et al., 2010; Evans
651 et al., 2020 and references therein), and iii) fluid inclusions within the shell structure (Gray et
652 al., 2023).

653 All of these relationships do possibly concern the ontogenetic PF calcite, since SEM
654 imaging of GOA specimens did not reveal secondary minerals or overgrowth on shell calcite

(Levy et al., 2023). Moreover, the enrichment of multiple trace elements across species suggests that secondary minerals are unlikely to be responsible for these trends. Discrepancies between Na/Ca in plankton tow versus core-top samples in the Red Sea (Mezger et al., 2018), as well as higher Na/Ca values measured by LA-ICP-MS compared to solution ICP-MS, have been linked to early diagenesis of Na-enriched phases like spines, ACC, or fluid inclusions (Gray et al., 2023). However, spines and ACC were ruled out for GOA samples, as all of the specimens had lost their spines before analysis and ACC was not detected via SEM. Given that most element/Ca in GOA shells are elevated relative to PF data from elsewhere, fluid inclusions may be a contributing factor (Gray et al., 2023). However, more research is required to investigate whether fluid inclusions are evident in PF shells from the GOA. In the absence of fluid inclusions, environmental changes, particularly during water column mixing, are considered to be the primary drivers of the observed trace element/Ca enrichments in the GOA.

5.2 Water column and sediment signal correlation: Implications to Paleoceanographic studies

Several element ratios (e.g., Al/Ca, Ti/Ca, Mn/Ca, Fe/Ca, Nd/Ca, U/Ca, Co/Ca, and Th/Ca) exhibit discrepancies between water column and core-top specimens (Fig. 8). Some, like Co/Ca, have lower values in surface sediment than the water column, while others, like Fe/Ca show higher values. Differences between sediment trap samples and core-top samples may stem from differential diagenetic processes that affect element/Ca in specimens taken from the water column and the sea floor. For example, diagenetic processes can lead to Mn accumulation and higher Mn/Ca in PF from the core top (McKenzie, 1980; Steiner et al., 2017). Conversely, core-top PF samples may show lower ratios due to the release of these metals into pore water over time (e.g., Co/Ca, Fig. 8i). This release can alter the elemental composition, potentially skewing paleoenvironmental reconstructions. Understanding these processes is crucial for accurately interpreting geochemical data from both sample types.

Despite the offsets of Al/Ca and Ti/Ca between core top and water column specimens, they nevertheless may be utilized to trace the origins of terrigenous inputs and identify periods of dust deposition in the geological record (Torfstein et al., 2017; Martinez-Garcia et al., 2011). Our data reveal significant seasonal excursions in Al/Ca and may demonstrate the use of Al/Ca and Ti/Ca in PF tests as proxies for dust or terrigenous input to the ocean (Fig. S3).

Core top element/Ca values that fall within the same range of values of the sediment trap specimens (Mg/Ca, Sr/Ca, B/Ca, Na/Ca, and Ba/Ca; Fig. 8) suggest that they could reflect water column conditions. The high temporal variability in many of these element/Ca data,

together with the varying PF population dynamics throughout the year (Fig. 2) may be considered when approaching PF from sediment cores. Seasonal trends in element/Ca are often obscured by the spring mixing event. However, exceptions to this are observed in Mg/Ca for *G. ruber albus* (Fig. 4; Levy et al., 2023) and B/Ca for *T. clarkei* (Fig. 5), where clear seasonal patterns emerge. A key limitation of reconstructing past environments from element/Ca in PF shells is the challenge of disentangling seasonal effects from other more episodic environmental signals. However, by identifying water column mixing events through positive element/Ca excursions and elevated ICV, which are evident across all species (Figs. 3-7), it may be possible to identify the time intervals over which environmental changes are reconstructed. This could allow for more accurate reconstructions of shifts in temperature, carbonate chemistry, and nutrient availability during specific mixing events, improving our understanding of past ocean conditions.

5.3 Regional comparison of geochemical conditions and PF element/Ca

The Mg/Ca, Al/Ca, and Na/Ca in PF from the GOA generally exceed those reported from other regions (Fig. 12b – 12e). Sr/Ca values, while reaching up to 2.2 mmol/mol during spring, have an average of 1.5 mmol/mol, consistent with previous studies (Fig. 12c; Kisakürek et al., 2008; Cleroux et al., 2008; Elderfield et al., 2002; Brown & Elderfield, 1996; Dissard et al., 2021). The high Mg/Ca range in the GOA versus typical open-ocean levels (0.5-5 μmol/mol) is attributed to elevated salinity (~ 41 compared to mean ocean values of 34.7), which is also evident by the high Na/Ca. The high Al/Ca values and their large variation may be attributed to the close proximity of GOA to terrestrial input. Ba/Ca in the GOA are significantly higher than the values reported in prior studies from Atlantic Ocean core samples and culture experiments (Hönisch et al., 2011; Lea & Boyle, 1991), representing a roughly ten-fold difference. These discrepancies likely stem from two factors: (1) higher salinity in the GOA increases the availability of cations and trace element incorporation into foraminifera shells, and (2) higher-resolution measurements here which reveal chamber-specific elemental ratios, where early chambers (F-1 and F-2) exhibit higher values than final chambers, leading to more accurate, chamber-level data compared to bulk measurements. Combined, these factors explain the elevated values relative to global reports.

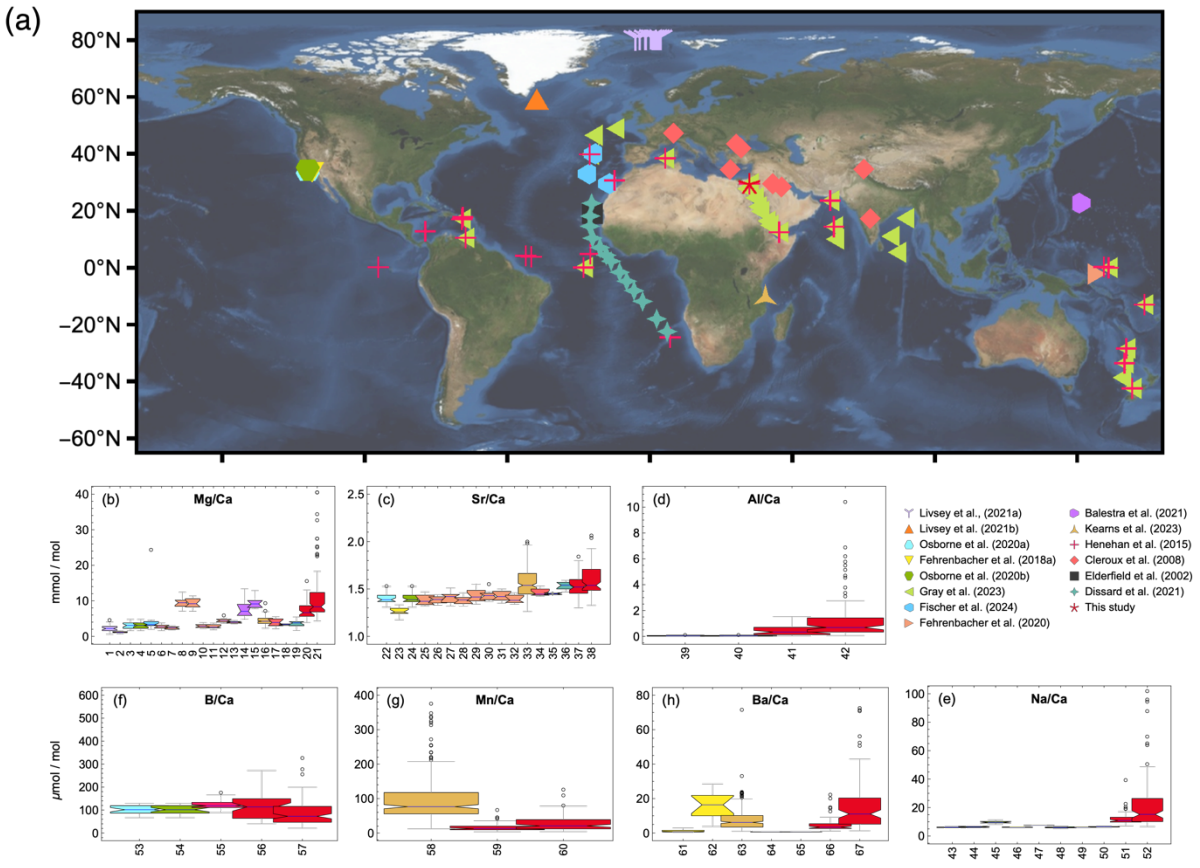

Figure 12. Global comparison of major and trace element-to-calcium ratios. (a) sample global map, (b) Mg/Ca of *N. pachyderma*, *G. bulloides*, *G. ruber white*, *N. dutertrei*, *O. universa*, *P. obliquiloculata*, *T. sacculifer* and *T. clarkei* derived from various sources (plankton tows/nets, sediment traps, cores) and measured by Laser Ablation (LA)-ICP-MS, solution-ICP-MS (SOL) and Electron micro-probe analyses (EPMA). (c) Sr/Ca of *G. bulloides*, *G. ruber white*, *N. dutertrei*, *O. universa*, *P. obliquiloculata*, *T. sacculifer* and *T. clarkei* derived from various sources (plankton tows/nets, sediment traps, cores) and measured by LA-ICP-MS and solution-ICP-MS. (d) Al/Ca of *G. bulloides*, *G. ruber white* and *T. clarkei* derived from sediment traps and measured by LA-ICP-MS. (e) Na/Ca of *G. ruber white* and *T. clarkei* from various sources (plankton tows/nets, sediment traps, cores and cultured samples) and measured by LA-ICP-MS and solution-ICP-MS. (f) B/Ca of *G. bulloides*, *G. ruber white* and *T. clarkei* derived from sediment traps and measured by LA-ICP-MS. (g) Mn/Ca of *G. ruber white* and *T. clarkei* derived from cores and sediment traps and measured by LA-ICP-MS. (h) Ba/Ca of *G. ruber white*, *N. dutertrei* and *T. clarkei* derived from various sources (plankton tows/nets, sediment traps, cores and cultured samples) and measured by LA-ICP-MS. See table 1 for detailed description of methods.

737

738

#	Element/Ca	Reference	Species	Collecting method	Measuring method
1	Mg/Ca	Livsey et al. (2021a)	*N. pachyderma*	Plankton tows / nets	LA
2	Mg/Ca	Livsey et al. (2021b)	*N. pachyderma*	Sediment traps	LA
3	Mg/Ca	Osborne et al. (2020)	*G. bulloides*	Sediment trap	LA
4	Mg/Ca	Osborne et al. (2020b)	*G. bulloides*	Sediment trap	LA
5	Mg/Ca	Fischer et al. (2024)	*G. ruber*	Plankton tows / nets	LA
6	Mg/Ca	Fehrenbacher et al. (2020)	*N. dutertrei*	Core	LA
7	Mg/Ca	Fehrenbacher et al. 2020	*N. dutertrei*	Core	SOL
8	Mg/Ca	Fehrenbacher et al. (2020)	*O. universa*	Core	LA
9	Mg/Ca	Fehrenbacher et al. (2020)	*O. universa*	Core	SOL
10	Mg/Ca	Fehrenbacher et al. (2020)	*P. obliquiloculata*	Core	LA
11	Mg/Ca	Fehrenbacher et al. (2020)	*P. obliquiloculata*	Core	SOL
12	Mg/Ca	Fehrenbacher et al. (2020)	*T. sacculifer*	Core	LA
13	Mg/Ca	Fehrenbacher et al. (2020)	*T. sacculifer*	Core	SOL
14	Mg/Ca	Balestra et al. (2021)	*O. universa*	Plankton tows / nets	EPMA

15	Mg/Ca	Balestra et al. (2022)	*O. universa*	Plankton tows / nets	EPMA
16	Mg/Ca	Kearns et al. (2023)	*G. ruber*	Core	LA
17	Mg/Ca	Cleroux et al. (2008)	*G. ruber*	Core	SOL
18	Mg/Ca	Elderfield et al. (2002)	*G. ruber*	Core	SOL
19	Mg/Ca	Dissard et al. (2021)	*T. sacculifer*	Plankton tows / nets	LA
20	Mg/Ca	This study	*G. ruber*	Sediment trap	LA
21	Mg/Ca	This study	*T. clarkei*	Sediment trap	LA
22	Sr/Ca	Osborne et al. (2020)	*G. Bulloides*	Sediment trap	LA
23	Sr/Ca	Fehrenbacher et al. (2018a)	*N. dutertrei*	Plankton tows / nets	LA
24	Sr/Ca	Osborne et al. (2020b)	*G. bulloides*	Sediment trap	LA
25	Sr/Ca	Fehrenbacher et al. (2020)	*N. dutertrei*	Core	LA
26	Sr/Ca	Fehrenbacher et al. (2020)	*N. dutertrei*	Core	SOL
27	Sr/Ca	Fehrenbacher et al. (2020)	*O. universa*	Core	LA
28	Sr/Ca	Fehrenbacher et al. (2020)	*O. universa*	Core	SOL
29	Sr/Ca	Fehrenbacher et al. (2020)	*P. obliquiloculata*	Core	LA
30	Sr/Ca	Fehrenbacher et al. (2020)	*P. obliquiloculata*	Core	SOL
31	Sr/Ca	Fehrenbacher et al. (2020)	*T. sacculifer*	Core	LA

32	Sr/Ca	Fehrenbacher et al. (2020)	*T. sacculifer*	Core	SOL
33	Sr/Ca	Kearns et al. (2023)	*G. ruber*	Core	LA
34	Sr/Ca	Cleroux et al. (2008)	*G. ruber*	Core	SOL
35	Sr/Ca	Elderfield et al. (2002)	*G. ruber*	Core	SOL
36	Sr/Ca	Dissard et al. (2021)	*T. sacculifer*	Plankton tows / nets	LA
37	Sr/Ca	This study	*G. ruber*	Sediment trap	LA
38	Sr/Ca	This study	*T. clarkei*	Sediment trap	LA
39	Al/Ca	Osborne et al. (2020)	*G. Bulloides*	Sediment trap	LA
40	Al/Ca	Osborne et al. (2020b)	*G. bulloides*	Sediment trap	LA
41	Al/Ca	This study	*G. ruber*	Sediment trap	LA
42	Al/Ca	This study	*T. clarkei*	Sediment trap	LA
43	Na/Ca	Gray et al. (2023)	*G. ruber*	Core	SOL
44	Na/Ca	Gray et al. (2023)	*G. ruber*	Cultured	SOL
45	Na/Ca	Gray et al. (2023)	*G. ruber*	Plankton tows / nets	LA
46	Na/Ca	Gray et al. (2023)	*G. ruber*	Plankton tows / nets	SOL
47	Na/Ca	Gray et al. (2023)	*G. ruber*	Sediment trap	LA
48	Na/Ca	Gray et al. (2023)	*G. ruber*	Sediment trap	SOL
49	Na/Ca	Gray et al. (2023)	*G. ruber mixed*	Core	SOL
50	Na/Ca	Gray et al. (2023)	*G. ruber sl*	Core	SOL

51	Na/Ca	This study	*G. ruber*	Sediment trap	LA
52	Na/Ca	This study	*T. clarkei*	Sediment trap	LA
53	B/Ca	Osborne et al. (2020)	*G. Bulloides*	Sediment trap	LA
54	B/Ca	Osborne et al. (2020b)	*G. Bulloides*	Sediment trap	LA
55	B/Ca	Henehan et al. (2015)	*G. ruber*	Core	SOL
56	B/Ca	This study	*G. ruber*	Sediment trap	LA
57	B/Ca	This study	*T. clarkei*	Sediment trap	LA
58	Mn/Ca	Kearns et al. (2023)	*G. ruber*	Core	LA
59	Mn/Ca	This study	*G. ruber*	Sediment trap	LA
60	Mn/Ca	This study	*T. clarkei*	Sediment trap	LA
61	Ba/Ca	Fehrenbacher et al. (2018a)	*N. dutertrei*	Cultured	LA
62	Ba/Ca	Fehrenbacher et al. (2018a)	*N. dutertrei*	Plankton tows / nets	LA
63	Ba/Ca	Kearns et al. (2023)	*G. ruber*	Core	LA
64	Ba/Ca	Hönisch et al. (2011)	*G. bulloides*	Cultured	SOL
65	Ba/Ca	Hönisch et al. (2011)	*O. universa*	Cultured	SOL
66	Ba/Ca	This study	*G. ruber*	Sediment trap	LA
67	Ba/Ca	This study	*T. clarkei*	Sediment trap	LA

739

740 Table 1: detailed description of the different species, measurement methods and sample
741 origin used for the compilation in figure 12. LA stands for Laser Ablation (LA)-ICP-MS,
742 SOL is solution-ICP-MS and EPMA is Electron micro-probe analyses.

6. Summary and conclusions:

We investigated the effects of inter-chamber variability on the proxy systematics in the hyper saline oligotrophic GOA using single chamber LA ICP-MS analysis measured on two flux-dominating planktic foraminifer (PF) species *G. ruber albus* and *T. clarkei* with its two phenotypes 'big' and 'encrusted'. We observed how element/Ca varies in PF chambers as a function of environmental changes in order to then be used as proxies for past oceanic and climatic reconstruction. The results show that some element/Ca exhibit temporal and seasonal variations related to environmental conditions in the water column such as Mg/Ca in *G. ruber albus* as a temperature proxy, and B/Ca in *T. clarkei* as a proxy of *p*H. Although other element/Ca values display more limited variability (e.g., Na/Ca) they may still be of use as paleo-proxies when combined in global calibration studies.

Water column mixing has been shown to have a significant effect of element/Ca positive excursions in the analyzed *G. ruber albus*, and two *T. clarkei* morphotypes, which may limit the use of some element ratios as proxies, or alternatively, be used as a proxy for water column mixing. Generally, pooled-mean values of element/Ca in the PF tests in the GOA are species-specific and element-specific, and are elevated compared to other regions (e.g., Mg/Ca, Al/Ca, Na/Ca). However, the final chamber F0 is different in comparison to the preceding chambers F-1 and F-2, suggesting that the element composition of F0 may be biased and unreliable in terms of recording environmental conditions.

Our findings indicate that high-resolution analytical techniques, such as LA ICP-MS enable studying single chamber compositions and variations. Although pooled mean values of specimens over various water depths are recommended for their incorporation as proxies, ICV can also be used as a tracer of environmental factors. Exploring different biochemical or physiological mechanisms which are responsible for the element/Ca variations between species and chambers are critical to shed light on how element/Ca are incorporated to the PF shells. Despite these limitations, the results provide valuable insights into the complex behavior of element/Ca in PF shells.

Data availability

Tabular supplementary data generated in this study can be found in the supplementary material.

774

775 Author contributions

776 NL, AT, and RS designed the study; NL, BS, UW, and KPJ, performed the measurements;
777 NL, NC, AT, and RS analyzed the data; NL, RS and AT wrote the manuscript draft; NL, RS,
778 AT and GH reviewed and edited the manuscript.

779

780 The authors declare that they have no conflict of interest.

781

782 Acknowledgments

783 We wish to acknowledge the IUI marine crew and B. Yarden for their assistance in field work
784 and sample handling. The National Monitoring Program are thanked for their support and
785 sharing results and E. Levy for fruitful discussions. We are thankful for the two reviewers,
786 Lennart de Nooijer and Takashi Toyofuku, whom their comments significantly improved this
787 manuscript. This work was supported by Israel Science Foundation grant 809/24 (to AT), a
788 Minerva PhD Fellowship stipend (to NL) and a scholarship from the Advance School for
789 Environmental Studies, HUJI (to NL).

790

791

References

Allen, K. A., Hönisch, B., Eggins, S. M., Haynes, L. L., Rosenthal, Y., & Yu, J. Trace element proxies for surface ocean conditions: A synthesis of culture calibrations with planktic foraminifera. *Geochim Cosmochim Ac*, *193*, 197-221. (2016).

Allen, K. A., Hönisch, B., Eggins, S. M., Yu, J., Spero, H. J., & Elderfield, H. Controls on boron incorporation in cultured tests of the planktic foraminifer Orbulina universa. *Earth Planet Sc Lett*, *309*(3-4), 291-301. (2011).

Allen, K. A., Hönisch, B., Eggins, S. M., & Rosenthal, Y. Environmental controls on B/Ca in calcite tests of the tropical planktic foraminifer species Globigerinoides ruber and Globigerinoides sacculifer. *Earth Planet Sc Lett*, *351*, 270-280. (2012).

Anderson, R. F., Bacon, M. P., & Brewer, P. G. Removal of230Th and231Pa from the open ocean. *Earth Planet Sc Lett*, *62*(1), 7-23. (1983).

Babila, T. L., Rosenthal, Y., & Conte, M. H. Evaluation of the biogeochemical controls on B/Ca of Globigerinoides ruber white from the Oceanic Flux Program, Bermuda. *Earth Planet Sc Lett*, *404*, 67-76. (2014).

Balestra, B., Rose, T., Fehrenbacher, J., Knobelspiesse, K. D., Huber, B. T., Gooding, T., & Paytan, A. In Situ Mg/Ca Measurements on Foraminifera: Comparison Between Laser Ablation Inductively Coupled Plasma Mass Spectrometry and Wavelength-Dispersive X-Ray Spectroscopy by Electron Probe Microanalyzer. *Geochem Geophy Geosy*, 22(2), e2020GC009449. (2021).

Bé, A. W., Hemleben, C., Anderson, O. R., Spindler, M., Hacunda, J., & Tuntivate-Choy, S. Laboratory and field observations of living planktonic foraminifera. *Micropaleontology*, 155-179. (1977).

Beasley, C., Kender, S., Giosan, L., Bolton, C. T., Anand, P., Leng, M. J., Nilsson-Kerr k., Ullmann C. V., Hesselbo S. P., & Littler, K. Evidence of a South Asian proto-monsoon during the Oligocene-Miocene transition. *Paleoceanogr Paleoclimatol*, *36*(9), e2021PA004278. (2021).

826 Berggren, W. A., Kent, D. V., Swisher, C. C., & Aubry, M. P. A revised Cenozoic
827 geochronology and chronostratigraphy. (1995).
828
829 Bertlich, J., Nürnberg, D., Hathorne, E. C., De Nooijer, L. J., Mezger, E. M., Kienast, M.,
830 Nordhausen S., Reichart G., Schönfeld J., & Bijma, J. Salinity control on Na incorporation into
831 calcite tests of the planktonic foraminifera Trilobatus sacculifer–evidence from culture
832 experiments and surface sediments. *Biogeosciences*, *15*(20), 5991-6018. (2018).
833
834 Bolton, A., Baker, J. A., Dunbar, G. B., Carter, L., Smith, E. G., & Neil, H. L. Environmental
835 versus biological controls on Mg/Ca variability in Globigerinoides ruber (white) from core top
836 and plankton tow samples in the southwest Pacific Ocean. *Paleoceanography*, *26*(2). (2011).

837 Brummer, G. J. A., & Kučera, M. Taxonomic review of living planktonic foraminifera. *J*
838 *Micropalaeontol*, *41*(1), 29-74. (2022).

839 Brown, S. J., & Elderfield, H. Variations in Mg/Ca and Sr/Ca ratios of planktonic foraminifera
840 caused by postdepositional dissolution: Evidence of shallow Mg-dependent
841 dissolution. *Paleoceanography*, *11*(5), 543-551. (1996).
842
843 Chang, F., Li, T., Xiong, Z., & Xu, Z. Evidence for sea level and monsoonally driven variations
844 in terrigenous input to the northern East China Sea during the last 24.3
845 ka. *Paleoceanography*, *30*(6), 642-658. (2015).
846
847 Chase, Z., Paytan, A., Beck, A., Biller, D., Bruland, K., Measures, C., & Sañudo-Wilhelmy, S.
848 Evaluating the impact of atmospheric deposition on dissolved trace-metals in the Gulf of
849 Aqaba, Red Sea. *Mar Chem*, *126*(1-4), 256-268. (2011).
850
851 Chernihovsky, N., Torfstein, A., & Almogi-Labin, A. Seasonal flux patterns of planktonic
852 foraminifera in a deep, oligotrophic, marginal sea: Sediment trap time series from the Gulf of
853 Aqaba, northern Red Sea. *Deep-Sea Res Pt I*, *140*, 78-94. (2018).
854
855 Chernihovsky, N., Almogi-Labin, A., Kienast, S. S., & Torfstein, A. The daily resolved
856 temperature dependence and structure of planktonic foraminifera blooms. *Sci Rep-Uk*, 10(1),
857 17456. (2020).

Cléroux, C., Cortijo, E., Anand, P., Labeyrie, L., Bassinot, F., Caillon, N., & Duplessy, J. C. Mg/Ca and Sr/Ca ratios in planktonic foraminifera: Proxies for upper water column temperature reconstruction. *Paleoceanography*, *23*(3). (2008).

Costa, K. M., Hayes, C. T., Anderson, R. F., Pavia, F. J., Bausch, A., Deng, F., Dutay, J., Geibert, W. Heinze, C., Henderson, G., Hillaire-Marcel, C., Hoffmann, S., Jaccard, S. L., Jacobel, A. W., Kienast, S. S., Kipp, L., Lerner, P., Lippold, J., Lund, D., Marcantonio, F., McGee, D., McManus, J. F., Mekik, F., Middleton, J. L., Missiaen, L., Not, C., Pichat, S., Robinson, L. F., Rowland, G. H., Roy-Barman, M., Tagliabue, A., Torfstein, A., Winckler, G., & Zhou, Y. 230Th normalization: New insights on an essential tool for quantifying sedimentary fluxes in the modern and Quaternary ocean. *Paleoceanogr Paleoclimatol*, *35*(2), e2019PA003820. (2020).

Davis, C. V., Fehrenbacher, J. S., Benitez-Nelson, C., & Thunell, R. C. Trace element heterogeneity across individual planktic foraminifera from the Modern Cariaco Basin. *J Foramin Res*, *50*(2), 204-218. (2020).

Dissard, D., Reichart, G. J., Menkes, C., Mangeas, M., Frickenhaus, S., & Bijma, J. Mg⁄Ca, Sr⁄Ca and stable isotopes from the planktonic foraminifera T. sacculifer: testing a multi-proxy approach for inferring paleotemperature and paleosalinity. *Biogeosciences*, *18*(2), 423-439. (2021).

Eggins, S., De Deckker, P., & Marshall, J. (2003). Mg/Ca variation in planktonic foraminifera tests: implications for reconstructing palaeo-seawater temperature and habitat migration. *Earth and Planetary Science Letters*, *212*(3-4), 291-306.

Elderfield, H., Vautravers, M., & Cooper, M. The relationship between shell size and Mg/Ca, Sr/Ca, δ18O, and δ13C of species of planktonic foraminifera. *Geochem Geophy Geosy*, *3*(8), 1-13. (2002).

Evans, D., Gray, W. R., Rae, J. W., Greenop, R., Webb, P. B., Penkman, K., Kröger, R., & Allison, N. Trace and major element incorporation into amorphous calcium carbonate (ACC) precipitated from seawater. *Geochim Cosmochim Ac*, *290*, 293-311. (2020).

Fehrenbacher, J., Marchitto, T., & Spero, H. J. Comparison of Laser Ablation and Solution-Based ICP-MS Results for Individual Foraminifer Mg/Ca and Sr/Ca Analyses. *Geochem Geophy Geosy*, *21*(12), e2020GC009254. (2020).

Fehrenbacher, Jennifer; Russell, Ann D; Davis, Catherine V; Spero, Howard J; Chu, Edward; Hönisch, Bärbel: Average barium/calcium ratios of cultured foraminifer specimens of Neogloboquadrina dutertrei, listed by experiment [dataset]. PANGAEA, https://doi.org/10.1594/PANGAEA.895792, (2018).

Fischer, A., Schiebel, R., Jochum, K. P., Heins, L., Arns, A. I., Aardema, H. M., Slagter, H., Calleja, M. L., Levy, N., Stoll, B., Weis, U., Repschläger, J., & Haug, G. H. Single chamber Mg/Ca analyses of Globigerinoides ruber for paleo-proxy calibration using femtosecond LA-ICP-MS. *Sci. Data*, *11*(1), 583. (2024).

Francois, R., Frank, M., Rutgers van der Loeff, M. M., & Bacon, M. P. 230Th normalization: An essential tool for interpreting sedimentary fluxes during the late Quaternary. *Paleoceanography*, *19*(1). (2004).

Fritz-Endres, T., Fehrenbacher, J. S., Russell, A. D., & Cynar, H. Increased productivity in the equatorial pacific during the deglaciation inferred from the Ba/Ca ratios of non-spinose planktic foraminifera. *Paleoceanogr Paleoclimatol*, *37*(12), e2022PA004506. (2022).

Ganor, E., & Foner, H. A. Mineral dust concentrations, deposition fluxes and deposition velocities in dust episodes over Israel. *J Geophys Res-Atmos*, *106*(D16), 18431-18437. (2001).

Ganssen, G. M., Peeters, F. J. C., Metcalfe, B., Anand, P., Jung, S. J. A., Kroon, D., & Brummer, G. J. Quantifying sea surface temperature ranges of the Arabian Sea for the past 20 000 years. *Clim Past*, 7(4), 1337-1349. (2011).

921 Geerken, E., De Nooijer, L. J., van Dijk, I., & Reichart, G. J. Impact of salinity on element
922 incorporation in two benthic foraminiferal species with contrasting magnesium
923 contents. *Biogeosciences*, 15(7), 2205-2218. (2018).
924
925 Gray, W. R., Evans, D., Henehan, M., Weldeab, S., Lea, D. W., Müller, W., & Rosenthal, Y.
926 Sodium incorporation in foraminiferal calcite: An evaluation of the Na/Ca salinity proxy and
927 evidence for multiple Na-bearing phases. *Geochim Cosmochim Ac*, 348, 152-164. (2023).
928
929 Gupta, B. K. S. *Modern foraminifera* (pp. 7-36). B. K. S. Gupta (Ed.). Dordrecht: Kluwer
930 Academic Publishers. (1999).

931 Haug, G. H., Gunther, D., Peterson, L. C., Sigman, D. M., Hughen, K. A., & Aeschlimann, B.
932 Climate and the collapse of Maya civilization. *Science*, 299(5613), 1731-1735. (2003).

933 Haynes, L. L., Hönisch, B., Holland, K., Rosenthal, Y., & Eggins, S. M. Evaluating the planktic
934 foraminiferal B/Ca proxy for application to deep time paleoceanography. *Earth Planet Sc*
935 *Lett*, 528, 115824. (2019).

936 Henehan, M. J., Foster, G. L., Rae, J. W., Prentice, K. C., Erez, J., Bostock, H. C., Marshall,
937 B. J., & Wilson, P. A. Evaluating the utility of B/C a ratios in planktic foraminifera as a proxy
938 for the carbonate system: A case study of Globigerinoides ruber. *Geochem Geophy*
939 *Geosy*, 16(4), 1052-1069. (2015).

940 Hönisch, B., Allen, K. A., Russell, A. D., Eggins, S. M., Bijma, J., Spero, H. J., Lea, D. W., &
941 Yu, J. Planktic foraminifers as recorders of seawater Ba/Ca. *Mar Micropaleontol*, 79(1-2), 52-
942 57. (2011).

943 Hönisch, B., Fish, C. R., Phelps, S. R., Haynes, L. L., Dyez, K., Holland, K., Fehrenbacher, J.,
944 Allen, K. A., Eggins, S. M., & Goes, J. I. Symbiont photosynthesis and its effect on boron
945 proxies in planktic foraminifera. *Paleoceanogr Paleoclimatol*, 36(10), e2020PA004022.
946 (2021).

947 Hupp, B. N., & Fehrenbacher, J. S. Intratest trace element variability in polar and subpolar
948 planktic foraminifera: Insights into vital effects, ontogeny, and biomineralization processes. *J*
949 *Foramin Res*, *54*(4), 355-374. (2024).

Israel National Monitoring Program (NMP) (http://www.iui-eilat.ac.il/Research/NMPmeteodata.aspx; Shaked and Genin. (2016).

Jochum, K. P., Jentzen, A., Schiebel, R., Stoll, B., Weis, U., Leitner, J., Repschläger, J., Nürnberg, D., & Haug, G. H. High-resolution Mg/Ca measurements of foraminifer shells using femtosecond LA-ICP-MS for paleoclimate proxy development. *Geochem Geophy Geosy*, *20*(4), 2053-2063. (2019).

Jochum, K. P., Stoll, B., Weis, U., Jacob, D. E., Mertz-Kraus, R., & Andreae, M. O. Non-matrix-matched calibration for the multi-element analysis of geological and environmental samples using 200 nm femtosecond LA-ICP-MS: A comparison with nanosecond lasers. *Geostand Geoanal Res*, *38*(3), 265-292. (2014).

Jonkers, L., De Nooijer, L. J., Reichart, G. J., Zahn, R., & Brummer, G. J. Encrustation and trace element composition of Neogloboquadrina dutertrei assessed from single chamber analyses–implications for paleotemperature estimates. *Biogeosciences*, *9*(11), 4851-4860. (2012).

Katz, M. E., Cramer, B. S., Franzese, A., Hönisch, B., Miller, K. G., Rosenthal, Y., & Wright, J. D. Traditional and emerging geochemical proxies in foraminifera. *J Foramin Res*, *40*(2), 165-192. (2010).

Katz, T., Ginat, H., Eyal, G., Steiner, Z., Braun, Y., Shalev, S., & Goodman-Tchernov, B. N. Desert flash floods form hyperpycnal flows in the coral-rich Gulf of Aqaba, Red Sea. *Earth Planet Sc Lett*, *417*, 87-98. (2015).

Kearns, L. E., Searle-Barnes, A., Foster, G. L., Milton, J. A., Standish, C. D., & Ezard, T. H. G. The influence of geochemical variation among Globigerinoides ruber individuals on Paleoceanographic reconstructions. *Paleoceanogr Paleoclimatol*, 38(4), e2022PA004549. (2023).

Kısakürek, B., Eisenhauer, A., Böhm, F., Garbe-Schönberg, D., & Erez, J. Controls on shell Mg/Ca and Sr/Ca in cultured planktonic foraminifera, Globigerinoides ruber (white). *Earth Planet Sc Lett*, *273*(3-4), 260-269. (2008).

Kucera, M. Chapter six planktonic foraminifera as tracers of past oceanic environments. Editor(s): Claude Hillaire–Marcel, Anne De Vernal, *Developments in marine geology*, Elsevier, 1, 213-262. ISBN 9780444527554, (2007).

Lea, D. W., & Boyle, E. A. Barium in planktonic foraminifera. *Geochim Cosmochim Ac*, 55(11), 3321-3331. (1991).

Levy, N., Torfstein, A., Schiebel, R., Chernihovsky, N., Jochum, K. P., Weis, U., Stoll, B., & Haug, G. H. Temperature calibration of elevated Mg/Ca in planktic Foraminifera shells from the hypersaline Gulf of Aqaba. *Geochem Geophy Geosy*, 24(7), e2022GC010742. (2023).

Livsey, Caitlin M; Kozdon, Reinhard; Bauch, Dorothea; Brummer, Geert-Jan A; Jonkers, Lukas; Orland, Ian; Hill, Tessa M; Spero, Howard J: In situ Magnesium/Calcium analyses by LA-ICP-MS in individual N. pachyderma shells from plankton tows deployed in the Fram Strait [dataset]. PANGAEA, https://doi.org/10.1594/PANGAEA.935527, (2021a).

Livsey, Caitlin M; Kozdon, Reinhard; Bauch, Dorothea; Brummer, Geert-Jan A; Jonkers, Lukas; Orland, Ian; Hill, Tessa M; Spero, Howard J: Mg/Ca analyses by LA-ICP-MS in N. pachyderma shells from Irminger Sea sediment traps [dataset]. PANGAEA, https://doi.org/10.1594/PANGAEA.935595, (2021b).

Martínez-Garcia, A., Rosell-Melé, A., Jaccard, S. L., Geibert, W., Sigman, D. M., & Haug, G. H. Southern Ocean dust–climate coupling over the past four million years. *Nature*, 476(7360), 312-315. (2011).

McKenzie, R. M. The adsorption of lead and other heavy metals on oxides of manganese and iron. *Soil Res*, *18*(1), 61-73. (1980).

Meeder, E., Mackey, K. R., Paytan, A., Shaked, Y., Iluz, D., Stambler, N., Rivlin, T., Post, A. F., & Lazar, B. Nitrite dynamics in the open ocean clues from seasonal and diurnal variations. *Mar Ecol Prog Ser*, *453*, 11-26. (2012).

Mesa-Fernández, J. M., Martínez-Ruiz, F., Rodrigo-Gámiz, M., Jiménez-Espejo, F. J., García, M., & Sierro, F. J. Paleocirculation and paleoclimate conditions in the western Mediterranean basins over the last deglaciation: New insights from sediment composition variations. *Global Planet Change*, 209, 103732. (2022).

Mezger, E. M., de Nooijer, L. J., Boer, W., Brummer, G. J. A., & Reichart, G. J. Salinity controls on Na incorporation in Red Sea planktonic foraminifera. *Paleoceanography*, 31(12), 1562-1582. (2016).

Mezger, E. M., de Nooijer, L. J., Siccha, M., Brummer, G. J., Kucera, M., & Reichart, G. J. Taphonomic and ontogenetic effects on Na/Ca and Mg/Ca in spinose planktonic foraminifera from the Red Sea. *Geochem Geophy Geosy*, *19*(11), 4174-4194. (2018).

Morard, R., Füllberg, A., Brummer, G. J. A., Greco, M., Jonkers, L., Wizemann, A., Weiner, A. K. M., Darling, K., Siccha, M., Ledevin, R., Kitazato, H., de Gardiel-Thoron, T., de Varges, C., & Kucera, M. Genetic and morphological divergence in the warm-water planktonic foraminifera genus Globigerinoides. *PloS one*, *14*(12), e0225246. (2019).

Naik, S. S., & Naidu, P. D. Boron/calcium ratios in Globigerinoides ruber from the Arabian Sea: Implications for controls on boron incorporation. *Mar Micropaleontol*, 107, 1-7. (2014).

Nürnberg, D., Bijma, J., & Hemleben, C. Assessing the reliability of magnesium in foraminiferal calcite as a proxy for water mass temperatures. *Geochim Cosmochim Ac*, *60*(5), 803-814. (1996).

Osborne, Emily B; Umling, Natalie E; Bizimis, Michael; Buckley, Wayne; Sadekov, Aleksey Y; Tappa, Eric; Marshall-Kesser, Brittney; Sautter, Leslie R; Thunell, Robert C: Boron to calcium ratios (B/Ca) of sediment trap collected planktonic foraminifera from the Santa Barbara Basin [dataset publication series]. PANGAEA, https://doi.org/10.1594/PANGAEA.91087, (2020a).

Osborne, Emily B; Umling, Natalie E; Bizimis, Michael; Buckley, Wayne; Sadekov, Aleksey Y; Tappa, Eric; Marshall-Kesser, Brittney; Sautter, Leslie R; Thunell, Robert C: Geochemistry of Globigerina Bulloides in Santa Barbara Basin measured by Laser Ablation [dataset]. PANGAEA, https://doi.org/10.1594/PANGAEA.912273, (2020b).

1047 Rebotim, A., Voelker, A. H., Jonkers, L., Waniek, J. J., Meggers, H., Schiebel, R., Fraile, I.,
1048 Schulz, M., & Kucera, M. Factors controlling the depth habitat of planktonic foraminifera in
1049 the subtropical eastern North Atlantic. *Biogeosciences*, 14(4), 827-859. (2017).

1050 Reichart, G. J., Jorissen, F., Anschutz, P., & Mason, P. R. (2003). Single foraminiferal test
1051 chemistry records the marine environment. *Geology*, *31*(4), 355-358.
1052
1053 Rosenthal, Y. Chapter nineteen elemental proxies for reconstructing cenozoic seawater
1054 paleotemperatures from calcareous fossils. Editor(s): Claude Hillaire–Marcel, Anne De
1055 Vernal, *Developments in Marine Geology*, Elsevier, 1, 765-797. ISBN 9780444527554,
1056 (2007).
1057
1058 Rosenthal, Y., Perron-Cashman, S., Lear, C. H., Bard, E., Barker, S., Billups, K., Bryan, M.,
1059 Delaney, M. L., deMenocal, P. B., Dwyer, G. S., Elderfield, H., German, C. R., Greaves, M.,
1060 Lea, D. W., Marchitto, T. M. Jr., Pak, D. K., Paradis, G. L., Russell, A. D., Schneider, R. R.,
1061 Scheiderich, K., Stott, L., Tachikawa, K., Tappa, E., Thunell, R., Wara, M., Weldeab, S., &
1062 Wilson, P. A. Interlaboratory comparison study of Mg/Ca and Sr/Ca measurements in
1063 planktonic foraminifera for paleoceanographic research. *Geochem Geophy Geosy 5*(4). (2004).
1064
1065 Sadekov, A., Eggins, S. M., De Deckker, P., Ninnemann, U., Kuhnt, W., & Bassinot, F. Surface
1066 and subsurface seawater temperature reconstruction using Mg/Ca microanalysis of planktonic
1067 foraminifera Globigerinoides ruber, Globigerinoides sacculifer, and Pulleniatina
1068 obliquiloculata. *Paleoceanography*, *24*(3). (2009).
1069
1070 Sadekov, A., Eggins, S. M., De Deckker, P., & Kroon, D. Uncertainties in seawater
1071 thermometry deriving from intratest and intertest Mg/Ca variability in Globigerinoides
1072 ruber. *Paleoceanography*, 23(1). (2008).
1073
1074 Schiebel, R., & Hemleben, C. *Planktic foraminifers in the modern ocean* (pp. 1-358). Berlin:
1075 Springer. (2017).
1076
1077 Shaked, Y., & Genin, A. Israel National Monitoring Program at the Gulf of Eilat Annual
1078 Report. (2016).
1079

1080 Spero, H. J., Mielke, K. M., Kalve, E. M., Lea, D. W. & Pak, D. K. Multispecies approach to
1081 reconstructing eastern equatorial Pacific thermocline hydrography during the past 360 kyr.
1082 *Paleoceanography*, 18, 1022 (2003).
1083
1084 Sprintall, J. & Tomczak, M. Evidence of the barrier layer in the surface layer of the tropics. *J*
1085 *Geophys Res-Oceans*, 97(C5), 7305-7316. (1992).
1086
1087 Steiner, Z., Lazar, B., Torfstein, A., & Erez, J. Testing the utility of geochemical proxies for
1088 paleoproductivity in oxic sedimentary marine settings of the Gulf of Aqaba, Red Sea. *Chem*
1089 *Geol*, *473*, 40-49. (2017).
1090
1091 Thirumalai, K., Richey, J. N., Quinn, T. M., & Poore, R. Z. Globigerinoides ruber morphotypes
1092 in the Gulf of Mexico: A test of null hypothesis. Scientific reports, 4(1), 6018.Torfstein, A.,
1093 Kienast, S. S., Yarden, B., Rivlin, A., Isaacs, S., & Shaked, Y. (2020). Bulk and export
1094 production fluxes in the Gulf of Aqaba, Northern Red Sea. *ACS Earth Space Chem*, 4(8), 1461-
1095 1479. (2014).
1096
1097 Torfstein, A., Teutsch, N., Tirosh, O., Shaked, Y., Rivlin, T., Zipori, A., Stein, M., Lazar, B.,
1098 & Erel, Y. Chemical characterization of atmospheric dust from a weekly time series in the
1099 north Red Sea between 2006 and 2010. *Geochim Cosmochim Ac*, *211*, 373-393. (2017).
1100
1101 Torres, M. E., Martin, R. A., Klinkhammer, G. P., & Nesbitt, E. A. Post depositional alteration
1102 of foraminiferal shells in cold seep settings: new insights from flow-through time-resolved
1103 analyses of biogenic and inorganic seep carbonates. *Earth Planet Sc Lett*, 299(1-2), 10-22.
1104 (2010).
1105
1106 Weldeab, S., Lea, D. W., Oberha¨nsli, H. & Schneider, R. R. Links between southwestern
1107 tropical Indian Ocean SST and precipitation over southeastern Africa over the last 17 kyr.
1108 *Palaeogeogr Palaeocl*. 410, 1–13 (2014).
1109
1110 Yu, J., Elderfield, H., & Hönisch, B. B/Ca in planktonic foraminifera as a proxy for surface
1111 seawater pH. *Paleoceanography*, 22(2). (2007).